// Weierstraß-Institut
für Angewandte Analysis und Stochastik

im Forschungsverbund Berlin e.V.

Preprint ISSN 0946 – 8633

Numerical experiments on the modulation theory for the nonlinear atomic chain

Wolfgang Dreyer[1], Michael Herrmann[2]

submitted: 26th May 2005

[1] Weierstrass Institute
for Applied Analysis and Stochastics
Mohrenstrasse 39
10117 Berlin
Germany
E-Mail: dreyer@wias-berlin.de

[2] Humboldt-Universität zu Berlin
Institut für Mathematik
Unter den Linden 6
10099 Berlin
Germany
E-Mail: michaelherrmann@math.hu-berlin.de

No. 1031
Berlin 2005

2000 *Mathematics Subject Classification.* 34K60, 35L65, 70F10, 74A25, 82C21.

Key words and phrases. atomic chain, modulation theory, traveling waves, thermodynamic limit.

This work was supported by the Deutsche Forschungsgemeinschaft (DFG) within the Priority Programme SPP 1095 *Analysis, Modeling and Simulation of Multiscale Problems*, see
`http://www.mathematik.uni-stuttgart.de/~mehrskalen`.

Edited by
Weierstraß-Institut für Angewandte Analysis und Stochastik (WIAS)
Mohrenstraße 39
10117 Berlin
Germany

Fax: + 49 30 2044975
E-Mail: preprint@wias-berlin.de
World Wide Web: http://www.wias-berlin.de/

Abstract

Modulation theory with periodic traveling waves is a powerful, but not rigorous tool to derive a thermodynamic description for the atomic chain. We investigate the validity of this theory by means of several numerical experiments.

1 Introduction

We consider an atomic chain with N identical particles, whose dynamics is given by a large system of ODEs. The focus of this study numerical investigation of the macroscopic limit $N \to \infty$ in case that the microscopic motion generates temperature on the macroscopic scale. This phenomenon leads on the macroscopic scale to a coupling of very high oscillations and slowly varying processes.

The atomic chain with nearest neighbour interaction, see Figure 1, consists of identical particles with unit mass. These are located on the real axis and are labeled by the index α. Let N be the number of particles, which may be finite (in this case $\alpha \in \{1, ..., N\}$) or even infinite (i.e. $\alpha \in \mathbb{Z}$). For any α, let $x_\alpha(t)$ and $v_\alpha(t) = \dot{x}_\alpha(t)$

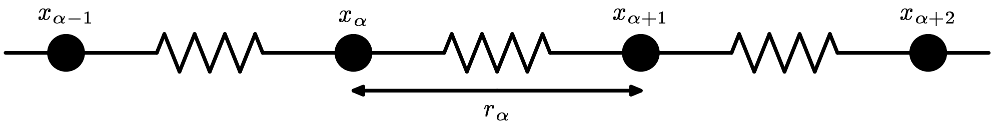

Figure 1: The atomic chain with nearest neighbour interaction.

denote the position and velocity, respectively, of the atom α at time t. Moreover, let $r_\alpha(t)$ be the distance of atoms $\alpha+1$ and α, i.e.

$$r_\alpha(t) \;\; := \;\; x_{\alpha+1}(t) - x_\alpha(t). \tag{1}$$

The dynamics in the atomic chain is governed by NEWTON's equations

$$\ddot{x}_\alpha(t) \;\; = \;\; \Phi'\Big(x_{\alpha+1}(t) - x_\alpha(t)\Big) - \Phi'\Big(x_\alpha(t) - x_{\alpha-1}(t)\Big), \tag{2}$$

where Φ is the atomic interaction potential. For our purposes it is convenient to consider distance and velocity as the independent variables. Eliminating x in (2) we find

$$\dot{r}_\alpha(t) \; = \; v_{\alpha+1}(t) - v_\alpha(t), \quad \dot{v}_\alpha(t) \; = \; \Phi'\Big(r_\alpha(t)\Big) - \Phi'\Big(r_{\alpha-1}(t)\Big). \tag{3}$$

The system (2) describes the evolution of the atomic chain on the *microscopic scale*, and thus we call t and α the *microscopic* time and particle index, respectively. If the particle number N is very large, we are not interested in the complete solution of (2), but rather in its thermodynamic properties. This means, we shall describe the evolution of the thermodynamic fields like mass density, momentum, pressure, temperature, energy, and entropy on a *macroscopic scale*.

Here we consider the macroscopic scale that results from the *hyperbolic scaling* (cf. Figure 2) as follows. We introduce the *scaling parameter* ε and define the macroscopic time $\overline{t}$ as well as the macroscopic particle index $\overline{\alpha}$ by

$$\overline{t} \;=\; \varepsilon t, \qquad \overline{\alpha} \;=\; \varepsilon\alpha. \tag{4}$$

Moreover, we define the macroscopic space $\overline{x}$ by $\overline{x} = \varepsilon x$. This fixes the scaling of

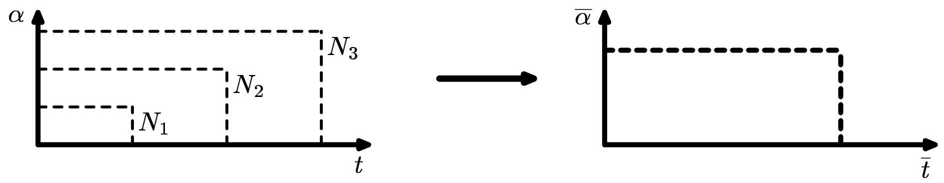

Figure 2: The hyperbolic scaling.

all other quantities: In particular, since there holds $x/t = \overline{x}/\overline{t}$ and $x/\alpha = \overline{x}/\overline{\alpha}$, the distance r as well as the velocity v remain unscaled.

The macroscopic description of the atomic chain is very complicated, if the atomic data exhibit oscillations on the microscopic scale, because in this case we have to describe the macroscopic evolution of temperature and entropy. A micro-macro transition is a theory, which can derive macroscopic evolution equations directly from (2). Unfortunately, no rigorous mathematical theory can do this without further assumptions. However, we can use modulation theory in order to establish a micro-macro transition at least formally.

The modulation theory used here, cf. Section 2.2 and the references therein, relies on periodic traveling waves of the atomic chain, because these can describe temperature in form of microscopic oscillations. A *traveling wave* is an exact solution of (2), which satisfies the ansatz

$$x_\alpha(t) \;=\; r\alpha + vt + \mathbb{X}\Big(k\alpha + \omega t\Big). \tag{5}$$

Here r, v, k and ω are four parameters and $\mathbb{X}$ is the *wave profile*. Motivated by its physical meaning we call r the *mean distance*, v the *mean velocity*, k the *wave number*, and ω the *frequency*. A micro-macro transition results, if we allow the parameters to vary on the macroscopic scale. The macroscopic evolution of the traveling wave parameter is governed by a system of *modulation equations*, which turns out to be

$$\frac{\partial}{\partial\,\overline{t}}\begin{pmatrix} r\\ v\\ k\\ S\end{pmatrix}\big(\overline{t},\,\overline{\alpha}\big) + \frac{\partial}{\partial\,\overline{\alpha}}\begin{pmatrix} -v\\ +p\\ -\omega\\ +g\end{pmatrix}\big(\overline{t},\,\overline{\alpha}\big) \;=\; 0. \tag{6}$$

These four equations may be interpreted as the macroscopic conservation laws of mass, momentum, wave number and entropy. Finally, the system (6) implies the conservation law of energy

$$\frac{\partial}{\partial \overline{t}}\Big(\frac{1}{2}v^2+U\Big)\left(\overline{t},\,\overline{\alpha}\right)+\frac{\partial}{\partial \overline{\alpha}}\big(vp+\omega g\big)\left(\overline{t},\,\overline{\alpha}\right) \;=\; 0. \tag{7}$$

The system (6) consists of four equations for seven variables. It is closed by the *equation of state* and a GIBBS equation, which both are closely related to travelling waves. The equation of state provides the internal energy U as function of the mean distance r, the wave number k and the entropy S. All other constitutive relations are in turn determined by the GIBBS equation, which reads

$$\mathrm{d}U \;=\; \omega\,\mathrm{d}S-p\,\mathrm{d}r-g\mathrm{d}k. \tag{8}$$

As mentioned above, the validity of the modulation system (6) with (8) for arbitrary potentials is not justified up to now. Only for very special potential some rigorous result are available (see [DHM04] and below). However, our numerical simulations indicate, that (6) and (8) describe in fact the macroscopic evolution of (2) in many situations.

All considerations which follow are restricted to convex interaction potentials, because we can establish the micro-macro transition only for these ones. In most cases we consider the TODA-potential ([Tod70, Tod81]),

$$\Phi(r) \;=\; \exp\left(1-r\right)+r-1, \tag{9}$$

which makes (2) completely integrable, cf. [Hén74, DM98]. However, the numerical results indicate that the integrability does not influence the validity of modulation theory, cf. Section 3.

In this study we consider two classes of initial value problems for (2). At first we consider finite chains with periodic boundary conditions. Secondly, we solve microscopic RIEMANN problems in the infinite chain. For this we start with a single jump discontinuity in the initial data, i.e. we set

$$r_\alpha(0)=\begin{cases} r_- & \text{for } \alpha<0\\ r_+ & \text{for } \alpha>0\end{cases},\qquad v_\alpha(0)=\begin{cases} v_- & \text{for } \alpha<0\\ v_+ & \text{for } \alpha>0\end{cases}, \tag{10}$$

where $r_\pm$ and $v_\pm$ are constants. As we will see, this kind of initial data generates self-similar solutions on the macroscopic scale, which consists of several waves like shocks and rarefaction waves.

The investigation of shocks in the atomic chain started already in 1978. In [HS78], HOLIAN and STRAUB considered the infinite chain with RIEMANN initial data $r_+ = r_-$ and $v_+ = v_- > 0$. They found by numerical experiments, that from these initial data there result two shock waves having sharp fronts and finite speeds $\pm c_{\mathrm{sp}}$ on the macroscopic scale. In particular, for large N the atoms remain at rest outside the space-time cone Ω, where

$$\Omega \quad = \quad \Big\{ \big(\bar{t}, \, \bar{\alpha} \big) \; : \; -c_{\mathrm{sp}} \, \bar{t} < \bar{\alpha} < +c_{\mathrm{sp}} \, \bar{t} \Big\}. \tag{11}$$

However, inside Ω the atoms perform high oscillations in form of a modulated wave train. Moreover, the behaviour in the center of Ω, that is

$$\Omega_{\mathrm{cent}} \quad = \quad \Big\{ \big(\bar{t}, \, \bar{\alpha} \big) \; : \; -c_{\mathrm{sp}} \, \bar{t} \ll \bar{\alpha} <\ll +c_{\mathrm{sp}} \, \bar{t} \Big\}, \tag{12}$$

depends on whether the value of v_- is smaller or larger than a critical value v_{crit}. While for $v_- < v_{\mathrm{crit}}$ all atoms within Ω_{cent} are at rest, for $v_- > v_{\mathrm{crit}}$ they perform binary oscillations, i.e. for large N then there holds

$$r_\alpha(t) \approx r_{\alpha+2}(t), \quad v_\alpha(t) \approx v_{\alpha+2}(t). \tag{13}$$

These numerical observations could later be justified rigorously for the Toda chain, see [HFM81], [VDO91], and [Kam91]. Finally, in [DKKZ96] the rarefaction problem for the Toda chain was solved. However, all these rigorous results use the complete integrability of (9), and do thus not cover other potentials. An explanation of the above mentioned phenomena in terms of modulation theory was proposed by Filip and Venakides. In [FV99] they study the modulation equations for small perturbations of the harmonic chain and determine the evolution of the modulated traveling wave by means of a numerical scheme.

In this study we present an approach for the numerical justification of modulation theory, which can be applied for all atomic interaction potentials, and which hopefully provides a better understanding of the underlying microscopic dynamics. Our main purposes are:

1. We perform detailed numerical studies on initial value problems for (2). In particular, we study the convergenceöf the numerical data for $N \to \infty$.

2. We compare the microscopic oscillations in the numerical data with the predictions coming from the traveling wave ansatz (5). We will identify many situations, in which the microscopic oscillations coincide with their macroscopic predictions.

3. We study the macroscopic evolution of the modulated traveling wave parameters as well as the other thermodynamic quantities.

This paper is organized as follows: We start with two numerical simulations to illustrate the basic problems and questions. In Section 2.1 we summarize some basic facts about traveling waves in the atomic chain. In particular, we introduce their thermodynamic properties, which become important in modulation theory. In 2.2 we proceed with a brief overview on the modulation theory as it is developed in [FV99, DHM04, Her04], and describe the equation of state and the GIBBS-equation.

Section 3 contains the numerical simulations: In 3.1 we explain the numerical methods and techniques that we have used, and in 3.2 and 3.3 we present the numerical results for several initial value problems. Finally, we discuss our result in Section 4.

Two numerical experiments

In order to motivate the considerations of the next section, we present at first two numerical simulations. The details of the implementation as well as the final interpretation of the results are, however, contained in Section 3.

Example $E1$

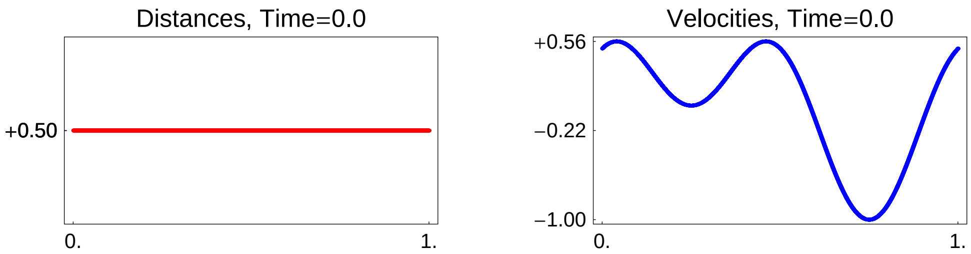

Figure 3: Cold initial data for Example $E1$: The atomic distances and velocities are plotted against the macroscopic particle index $\overline{\alpha}$. ◇

In the first example we initialize the atomic chain with *cold* initial data. This means we choose two functions r_{ini} and v_{ini}, which depend on $\overline{\alpha}$, and set

$$r_\alpha(0) = r_{\text{ini}}(\varepsilon\alpha), \qquad v_\alpha(0) = v_{\text{ini}}(\varepsilon\alpha) \qquad \text{for } \alpha = 1...N, \tag{14}$$

where N is a fixed particle number and $\varepsilon = 1/N$ is the scaling parameter. In this example r_{ini} and v_{ini} are given by

$$r_{\text{ini}}(\overline{\alpha}) = 0.5 \quad \text{and} \quad v_{\text{ini}}(\overline{\alpha}) = \frac{1}{2}\sin(2\pi\overline{\alpha}) + \frac{1}{2}\cos(4\pi\overline{\alpha}). \tag{15}$$

We refer to the ansatz (14) as *cold* initial data, because for large N there are no oscillations on the microscopic scale, see Figure 14. From the physical point of view this absence of oscillations means that there is no *temperature*.

Next we solve NEWTON's equations (2) for different particle numbers N, whereas we close (2) by imposing periodic boundary conditions, i.e. we suppose $r_{N+1}(t) = r_1(t)$ and $v_0(t) = v_N(t)$. We compute the solution in a fixed *macroscopic* time interval

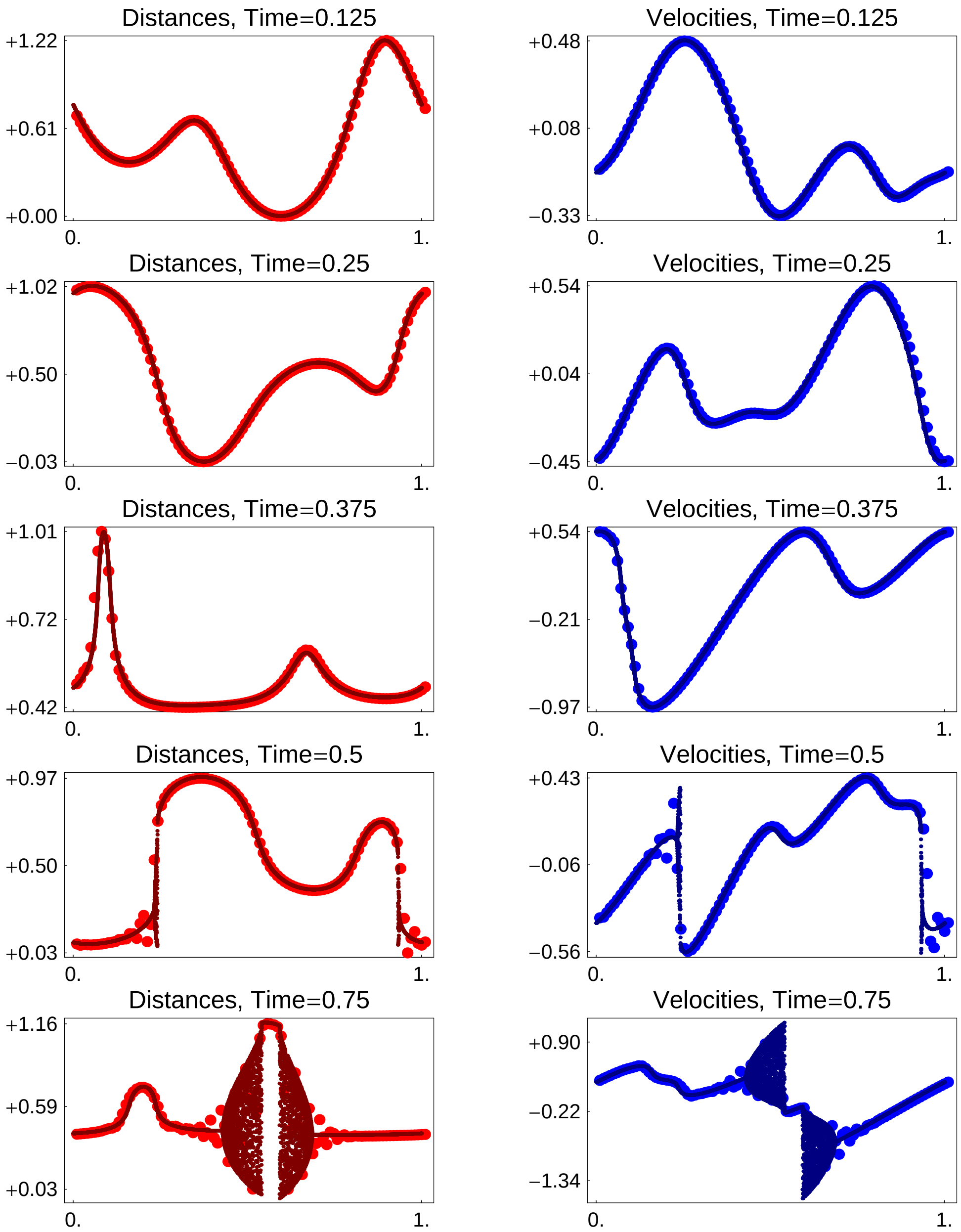

Figure 4: The atomic distances and velocities for Example $E1$: For several macroscopic times $\overline{t}$ the data are plotted against $\overline{\alpha}$, Bright and dark colors correspond to $N = 100$ and $N = 16000$, respectively. At $\overline{t} \approx 0.5$ the atomic data start to oscillate on the microscopic scale, so that temperature is created. $\diamond$

$[0, \overline{t}_{\text{end}}]$ with $\overline{t}_{\text{end}} = 0.7$. The hyperbolic scaling then determines the corresponding microscopic time by $t_{\text{end}} = N\overline{t}_{\text{end}}$.

The atomic distances and velocities for later times are shown in Figure 4, where bright and dark colors correspond to $N = 100$ and $N = 16000$, respectively. Note that all data are plotted against the macroscopic particle index $\overline{\alpha}$. The numerical results can be interpreted as follows:

1. Until $\bar{t} \approx 0.5$ the atomic data remain cold and converge for $N \to \infty$ to macroscopic functions, so that in the limit we obtain in any point $\left(\bar{t}, \bar{x}\right)$ unique values for distance and velocity.

2. At time $\bar{t} \approx 0.5$ the atomic data start to oscillate. These oscillations can be interpreted as temperature. From the mathematical point of view the oscillations prevent that the limit $N \to \infty$ can be described completely in terms of functions, but only by means of measures. Even if we are interested only in the *mean distance* and the *mean velocity*, the oscillations remain important because they dissipate energy, i.e. they transform macroscopic energy into internal energy.

Example $E2$

Here we study the evolution of initial data with temperature, i.e. with microscopic oscillations, by setting

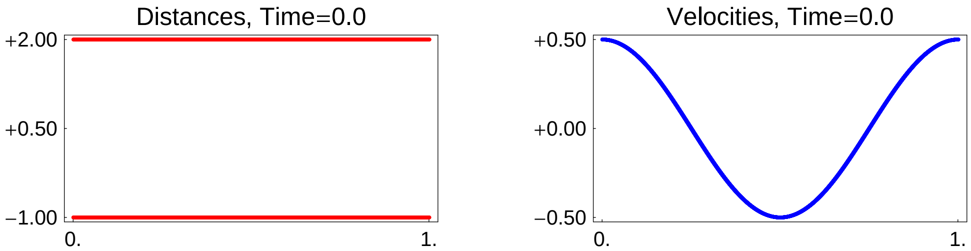

Figure 5: Initial data with temperature for Example $E2$, plotted against $\overline{\alpha}$. ⋄

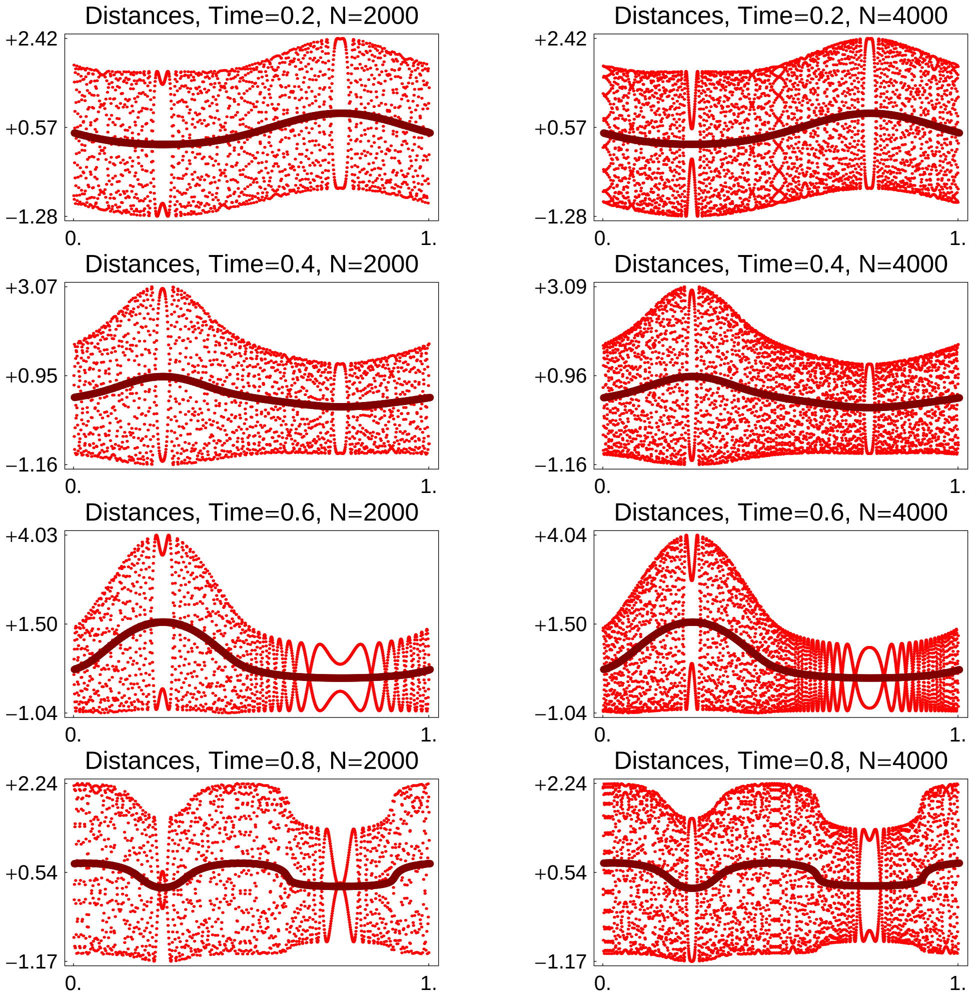

Figure 6: Atomic distances for example $E2$, plotted against $\overline{\alpha}$. Different rows correspond to different macroscopic times, left and right column to $N = 2000$ and $N = 4000$, respectively. Compare with the atomic velocities in Figure 7. ⋄

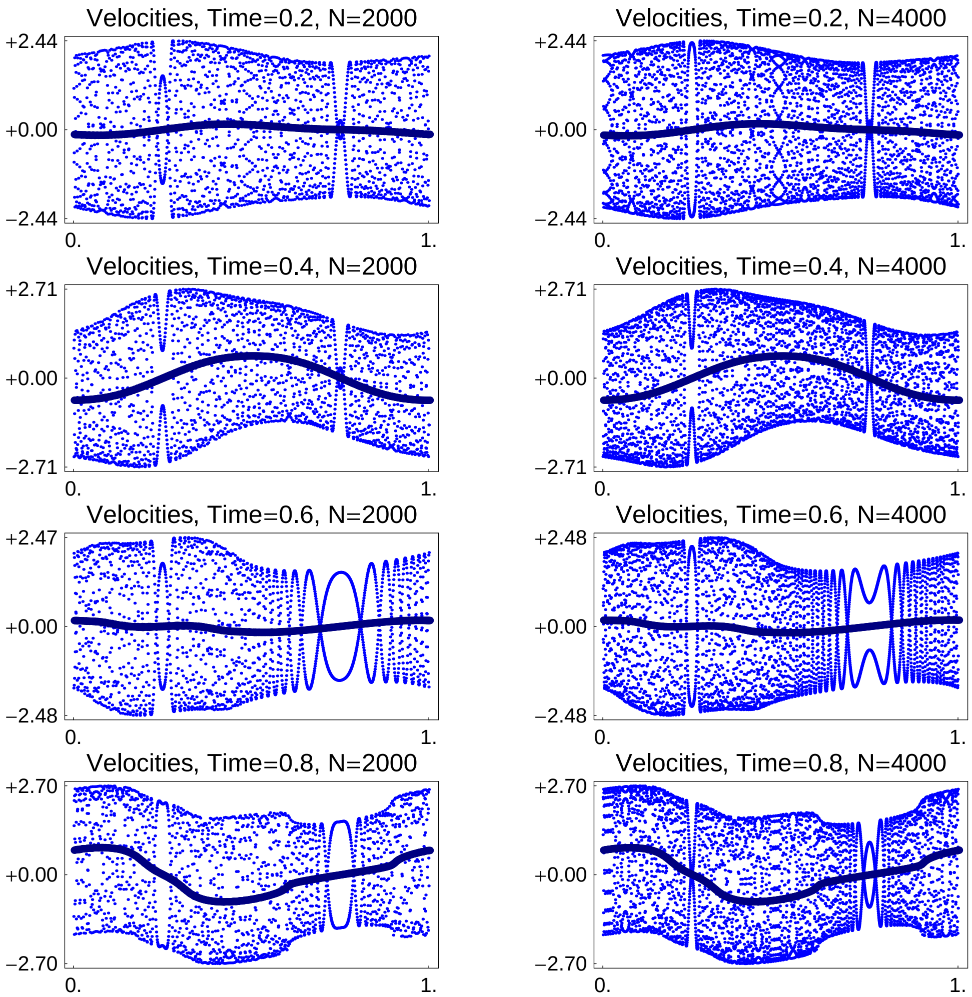

Figure 7: Atomic velocities for Example $E2$. $\diamond$

$$v_\alpha(0) \;=\; \frac{1}{2}\cos\left(2\pi\varepsilon\alpha\right), \qquad r_\alpha(0) \;=\frac{1}{2}-\frac{3}{2}(-1)^\alpha. \tag{16}$$

We observe in Figure 5 that the initial atomic distances are oscillating on the microscopic scale, and we mention that for all $\overline{t} > 0$ the velocities become likewise oscillating. In Section 3 we identify this kind of initial data as *modulated binary oscillations*.

Similarly as in the previous example, we have solved NEWTON's equations for different particle numbers but for fixed macroscopic final time $\overline{t}_{\rm end} = 0.8$. Then we have plotted the resulting atomic data against $\overline{\alpha}$, see the Figures 6 and 7. Note that the data for $N = 2000$ and $N = 4000$ are arranged in the left and right column, respectively. We see that the atomic data are oscillating on the microscopic scale. Therefore we shall describe them by measures and not by functions. The dark colored curves in the Figures 6 and 7 represent the local mean values of the atomic

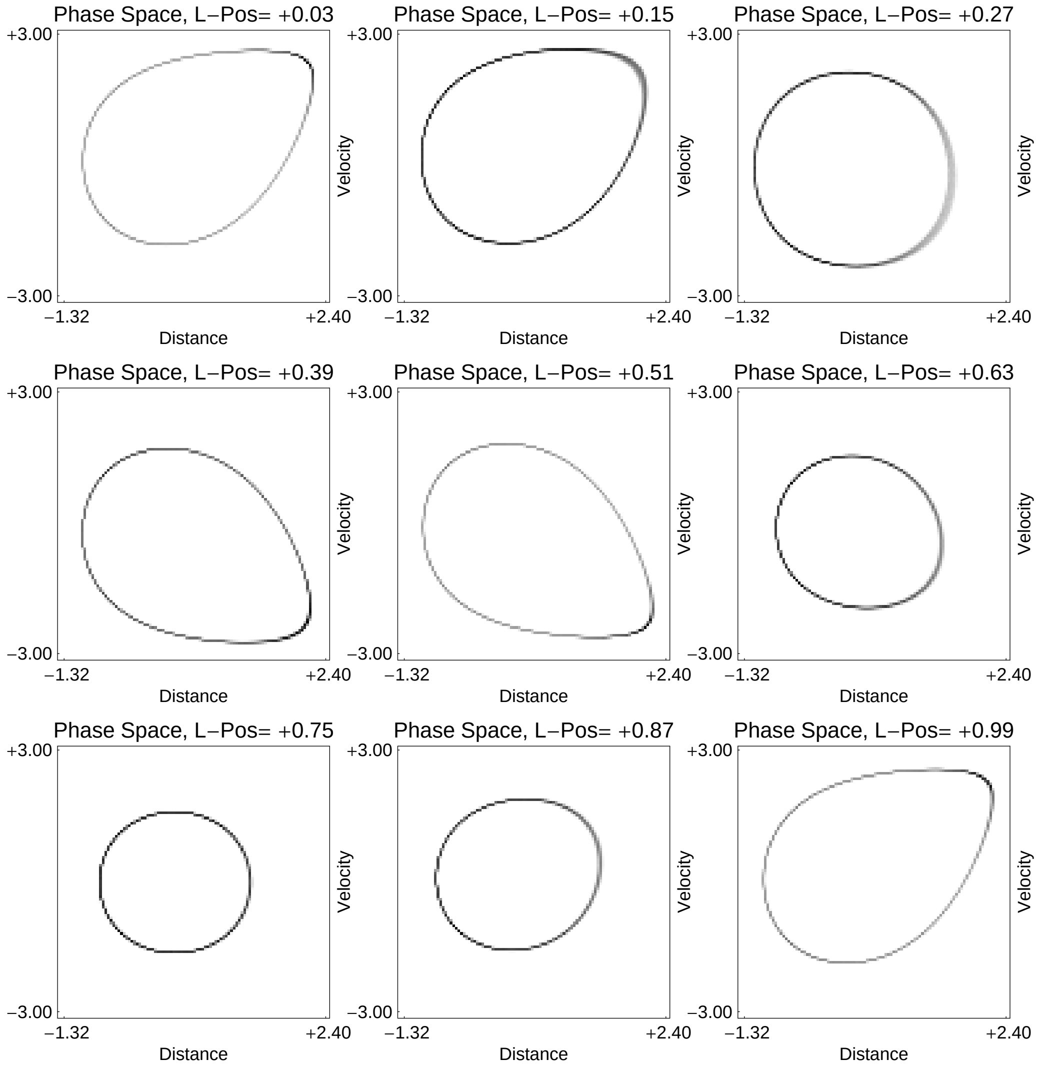

Figure 8: Local distribution functions in the microscopic phase space for Example $E2$. $\diamond$

data, whose computation we will describe in Section 3. However, we observe almost the same structure of oscillations for all particles numbers. For that reason we can expect that the atomic data converge for $N \to \infty$ in the sense of YOUNG-measures to a unique limit measure. Moreover, the local mean values converge for $N \to \infty$ in the sense of functions.

In the last step we investigate the fine structure of the microscopic oscillations in more detail. We fix a macroscopic point $Q_0 = \big(\overline{t}_0,\, \overline{\alpha}_0\big)$ and consider the *window* $\mathcal{F}_{Q_0}$ around $\big(\overline{t}_0,\, \overline{\alpha}_0\big)$, which consists of all microscopic points close to Q. This reads

$$\mathcal{F}_{Q_0} \;=\; \big\{(t,\, \alpha)\;:\;(\varepsilon t,\, \varepsilon\alpha) \approx \big(\overline{t}_0,\, \overline{\alpha}_0\big)\big\}. \tag{17}$$

In particular, the window $\mathcal{F}_{Q_0}$ is very small in macroscopic units, but contains a large number of time steps as well as particles. Next we evaluate the distribution functions of the atomic data within $\mathcal{F}_{Q_0}$, see Section 3 for the details. For our purposes it is convenient to consider the distribution functions in the *microscopic phase space*, which is the plane spanned by distance and velocity.

Figure 8 contains density plots of the distribution functions in nine selected windows, where Black and White indicate a high and low, respectively, probability for finding a particle. All windows are located at $\overline{t} = 0.9$; the corresponding $\overline{\alpha}$-coordinate can be read off in Figure 8 from the headlines as "L-pos". In Figure 8 we see (i) that the support of every distribution functions is contained in closed curves, and (ii) that the distribution functions vary on the macroscopic scale.

In what follows we have mainly three objectives:

1. First we derive a suitable descriptions for microscopic oscillations similar to those from Figure 8. In particular, it turns out that such oscillations correspond to traveling waves, and that they depend only on four parameters.
2. In Section 2.2 we introduce the modulation equations, which govern the macroscopic evolution of the traveling wave parameter.
3. Since there is no rigorous justification of the modulation equations, except for some very special cases, see [DHM04, Her04], we perform detailed numerical experiments in order to investigate their validity.

2 Foundations

2.1 Periodic Traveling Waves

In this section we summarize the most important properties of traveling waves. At first we mention that the traveling wave profile $\mathbb{X}$ in (5) is determined by a difference-differential equation. Plugging the ansatz (5) into (2) we find

$$\omega^2 \frac{\mathrm{d}^2}{\mathrm{d}\varphi^2}\mathbb{X}(\varphi) \;=\; \Phi'\Big(r + \mathbb{X}(\varphi + k) - \mathbb{X}(\varphi)\Big) - \Phi'\Big(r + \mathbb{X}(\varphi) - \mathbb{X}(\varphi - k)\Big), \quad (18)$$

where $\phi = k\alpha + \omega t$ denotes the *phase*. Note that v does not appear in (18), because (2) is invariant under GALILEI transformations.

Here we do not address the non-trivial existence problem for solutions of (18), but refer to the literature, as for instance [FW94, AG96, FP99, FV99, PP00]. In order to describe a micro-macro transition with temperature we use solely periodic traveling waves, because they can describe the microscopic oscillations from the numerical simulations. Since the periodicity length φ_{per} of traveling waves can be chosen arbitrarily, we always suppose $\varphi_{\mathrm{per}} = 1$.

Next we describe the thermodynamic properties of traveling waves, because they determine the equation of state, which provides the closure for (6). To this end we introduce two further 1-periodic profile functions $\mathbb{R}$ and $\mathbb{V}$ by

$$\mathbb{V}(\varphi) = \frac{\mathrm{d}}{\mathrm{d}\varphi}\mathbb{X}(\varphi), \qquad \mathbb{R}(\varphi) = \mathbb{X}(\varphi + k/2) - \mathbb{X}(\varphi - k/2), \tag{19}$$

$\mathbb{R}$ and $\mathbb{V}$ are related to the oscillating atomic distances and velocity in an exact traveling wave via

$$r_\alpha(t) \;=\; r + \mathbb{R}(k\alpha + \omega t + k/2), \quad v_\alpha(t) \;=\; v + \omega\mathbb{V}(k\alpha + \omega t). \tag{20}$$

Most of the thermodynamic quantities are defined as mean values of the oscillating atomic data in a traveling wave:

$$\begin{aligned}
W &= \int_0^1 \Phi(r + \mathbb{R}(\varphi))\,\mathrm{d}\varphi && \text{specific internal potential energy density,}\\
p &= -\int_0^1 \Phi'(r + \mathbb{R}(\varphi))\,\mathrm{d}\varphi && \text{pressure = negative specific force density,}\\
K &= \frac{\omega^2}{2}\int_0^1 \mathbb{V}(\varphi)^2\,\mathrm{d}\varphi && \text{specific internal kinetic energy density,}
\end{aligned}$$

and

$$\begin{aligned}
T &= 2K && \text{kinetic temperature,}\\
F &= K - W && \text{specific internal action density,}\\
U &= K + W && \text{specific internal energy density,}\\
E &= \frac{1}{2}v^2 + U && \text{specific energy density.}
\end{aligned}$$

Note that all these quantities are constants when we consider exact traveling waves. However, in modulation theory they become fields in $\overline{t}$ and $\overline{\alpha}$, whose evolution is described by the modulation system (6).

There are other important thermodynamic quantities, which are not related directly to the atomic data, because they have no microscopic counterpart. It turns out that S and g, which are defined by

$$\begin{aligned}
S &:= \omega\int_0^1 \mathbb{V}(\varphi)^2\;\mathrm{d}\varphi,\\
g &:= -\int_0^1 \frac{1}{2}(\mathbb{V}(\varphi + k/2) + \mathbb{V}(\varphi - k/2))\;\Phi'(r + \mathbb{R}(\varphi))\;\mathrm{d}\varphi
\end{aligned} \tag{21}$$

can be interpreted as the macroscopic *entropy density* and *entropy flux*, respectively, cf. [DHM04, Her04].

2.2 Summary on modulation theory

Modulation theory is a powerful tool which provides an effective dynamical model on the macroscopic scale. We mention that modulation theory was developed in the context of partial differential equations, see the examples in [Whi74], and that it can be applied to other discrete systems, see for instance [HLM94].

The modulation theory for the atomic chain with hyperbolic scaling relies on periodic traveling waves, and leads to a macroscopic theory, which is complex enough to describe the generation of temperature as well as the transport of heat. There are other reasonable scalings for the atomic chain, for which a macroscopic modulation equation is known. Examples are the KdV-scaling in [FP99, SW00], which leads to a macroscopic KORTEWEG-DE VRIES equations, and the NSE-scaling in [GM04b, GM04a], where the macroscopic evolution is governed by the nonlinear SCHROEDINGER equation.

The main idea behind modulation theory is the construction of *approximate* solutions of the microscopic system (5) by allowing the traveling wave parameter to vary on the macroscopic scale. A *modulated traveling waves* is an approximate solution of NEWTON's equations which satisfies the following ansatz for the atomic positions:

$$x_\alpha(t) \quad = \quad \frac{1}{\varepsilon}X(\varepsilon t,\, \varepsilon\alpha) + \tilde{\mathbb{X}}\Big(\varepsilon t,\, \varepsilon\alpha;\, \frac{1}{\varepsilon}\Theta(\varepsilon t,\, \varepsilon\alpha)\Big) + \mathcal{O}(\varepsilon), \tag{22}$$

where X and Θ are two macroscopic functions. The modulated traveling waves parameters are now fields in $\overline{t}$ and $\overline{\alpha}$. They are determined as derivatives of X and Θ via

$$v\big(\overline{t},\, \overline{\alpha}\big) = \frac{\partial X}{\partial \overline{t}}\big(\overline{t},\, \overline{\alpha}\big), \qquad r\big(\overline{t},\, \overline{\alpha}\big) = \frac{\partial X}{\partial \overline{\alpha}}\big(\overline{t},\, \overline{\alpha}\big), \tag{23}$$

$$\omega\big(\overline{t},\, \overline{\alpha}\big) = \frac{\partial \Theta}{\partial \overline{t}}\big(\overline{t},\, \overline{\alpha}\big), \qquad k\big(\overline{t},\, \overline{\alpha}\big) = \frac{\partial \Theta}{\partial \overline{\alpha}}\big(\overline{t},\, \overline{\alpha}\big). \tag{24}$$

The function $\tilde{\mathbb{X}}$ serves to model the microscopic oscillations and provides the link to traveling waves. In particular,

$$\tilde{\mathbb{X}}\big(\overline{t},\, \overline{\alpha};\, \varphi\big) \quad = \quad \mathbb{X}\big(r\big(\overline{t},\, \overline{\alpha}\big),\, v\big(\overline{t},\, \overline{\alpha}\big),\, k\big(\overline{t},\, \overline{\alpha}\big),\, \omega\big(\overline{t},\, \overline{\alpha}\big);\, \varphi\big), \tag{25}$$

where $\mathbb{X}$ is a family of traveling wave profiles, which depends on the parameters r, v, k, and ω, as well as on the phase variable φ. In order to ensure that (22) yields in fact approximate solutions of (2), we cannot choose X and Θ arbitrary, but we have to satisfy some restrictions. By means of the *Principle of least action* it can be shown, but only formally, that the modulated parameters have to satisfy the modulation equations (6), see [FV99, DHM04, Her04] for the details.

In [DHM04] it is proved, that any such family $\mathbb{X}$ of traveling waves provides an equation of state $F = F(r,\, k,\, \omega)$ together with the following variant of the GIBBS equation

$$\mathrm{d}F \quad = \quad S\,\mathrm{d}\omega \;+\; p\,\mathrm{d}r \;+\; g\,\mathrm{d}k. \tag{26}$$

By means of the formal Legendre transform $S\mathrm{d}\omega = \mathrm{d}\omega S - \omega \mathrm{d}S$ we can replace the frequency ω by the entropy S, and there result $U = U(r,\, k,\, S)$ as equation of state and the GIBBS equation (8), see [DHM04].

Up to now the modulation theory is not completely understood, because some serious problems remain open:

1. In modulation theory we suppose that traveling waves depend on four independent parameters. It was proved in [FV99] that for convex interaction potentials there always exists families of traveling with four independent parameters. However, presently there is no corresponding uniqueness result.

2. There is no rigorous result which guaranties (i) that the equation of state is unique, and (ii) that the modulations system is hyperbolic or even strictly hyperbolic.

3. For almost all potentials the equation of state is not known explicitly.

4. There is no rigorous justification of the modulation system, except for the harmonic chain and the hard-sphere model (see [Mie05, DHM04, Her04]).

Next we describe the modulation theory for *cold* data. We say the atomic data are *cold*, if there exist two macroscopic fields r and v, such that

$$r_\alpha(t) \;=\; r(\varepsilon t,\, \varepsilon\alpha), \quad v_\alpha(t) \;=\; v(\varepsilon t,\, \varepsilon\alpha). \tag{27}$$

Note that here k and ω have no meaning, because the temperature is zero. We can read off from (3) the corresponding macroscopic evolution directly, namely

$$\frac{\partial}{\partial \overline{t}} \begin{pmatrix} r \\ v \end{pmatrix} (\overline{t},\, \overline{\alpha}) - \frac{\partial}{\partial \overline{\alpha}} \begin{pmatrix} v \\ \Phi'(r) \end{pmatrix} (\overline{t},\, \overline{\alpha}) \;=\; 0. \tag{28}$$

This nonlinear and hyperbolic system is equivalent to the first two equations of (6), if we use $U = \Phi(r)$ as the equation of state.

A further special case is the harmonic chain, where

$$\Phi(d) \;=\; c_0 + c_1\, d + \frac{c_2}{2}\, d^2, \tag{29}$$

for which all traveling waves can be given explicitly, cf. [DHM04]. In particular, there results the following equation of state

$$U(r,\, k,\, S) \;=\; c_0 + c_1 r + \frac{1}{2} c_2 r^2 + \omega(k) S. \tag{30}$$

Note that the frequency ω is related to the wave number k by the *harmonic dispersion relation*

$$\omega(k) \;=\; \sqrt{c_2}\, \sin{(\pi k)}/\pi. \tag{31}$$

According to (6) and (30), the modulation equations for the harmonic chain read

$$\frac{\partial}{\partial \bar{t}} \begin{pmatrix} r \\ v \\ k \\ S \end{pmatrix} (\bar{t}, \bar{\alpha}) - \frac{\partial}{\partial \bar{\alpha}} \begin{pmatrix} v \\ r \\ \omega(k) \\ \omega'(k) S \end{pmatrix} (\bar{t}, \bar{\alpha}) \quad = \quad 0, \tag{32}$$

and are thus decoubled into two 2×2-systems.

3 Numerical Simulations

In this section we present numerical simulations in order to investigate the validity of the micro-macro transition and the modulation equations (6). To this end we study the following two classes of initial value problems:

1. Class S: Smooth initial data and periodic boundary conditions.
2. Class R: Microscopic RIEMANN problems.

In almost all simulation the atomic interaction potential is given by the TODA potential (9). However, other nonlinear and convex interaction potentials lead to similar results (see for instance Example $S2$), so that integrability seems to be not important in the thermodynamic limit.

3.1 Methods and Techniques

Numerical integrator, initial data and time steps

For the numerical integration of (2) we use the VERLET method, which is a symplectic integrator of second order, see [HLW02, SYS97]. The one-step formulation of the VERLET method reads

$$x_\alpha^{(i+1)} \quad = \quad x_\alpha^{(i)} + h\, v_\alpha^{(i)} + \frac{h^2}{2} p_\alpha^{(i)}, \tag{33}$$

$$v_\alpha^{(i+1)} \quad = \quad v_\alpha^{(i)} + \frac{h}{2} \big(p_\alpha^{(i+1)} + p_\alpha^{(i)} \big), \tag{34}$$

$$p_\alpha^{(i)} \quad = \quad \Phi' \Big(x_{\alpha+1}^{(i)} - x_\alpha^{(i)} \Big) - \Phi' \Big(x_\alpha^{(i)} - x_{\alpha-1}^{(i)} \Big). \tag{35}$$

Here $h = \Delta t$ is the microscopic time step size, and the upper index (i) denotes the ith time step. Recall that for given N the particle index α takes values in $\{1...N\}$.

For initial value problems of the class S we use periodic boundary conditions, i.e. we impose

$$x_0^{(i)} = x_N^{(i)} - L \quad \text{and} \quad x_{N+1}^{(i)} = x_1^{(i)} + L, \tag{36}$$

where the value of the *total length* L is fixed by the initial data.

We cannot expect the modulation theory to be valid for all classes of atomic initial data, but we have to restrict our considerations to initial data in form of modulated traveling waves. For the sake of simplicity we consider solely initial data in form of modulated *binary oscillations*. Modulated binary oscillations are modulated traveling waves, in which the wave number is not modulated, but constant with value 1/2. These have the advantage that the explicit knowledge of the profile functions is not necessary. In order to initialize the chain with modulated binary oscillations, we choose four macroscopic functions $r^{\,\mathrm{odd}}$, $r^{\,\mathrm{even}}$ and $v^{\,\mathrm{odd}}$, $v^{\,\mathrm{even}}$, which all depend only on $\overline{\alpha}$, and we set

$$r_\alpha(0) \;=\; \begin{cases} r_{\mathrm{ini}}^{\mathrm{odd}}(\varepsilon\alpha) & \text{falls} \quad \alpha \text{ odd,} \\ r_{\mathrm{ini}}^{\mathrm{even}}(\varepsilon\alpha) & \text{falls} \quad \alpha \text{ even,} \end{cases} \tag{37}$$

$$v_\alpha(0) \;=\; \begin{cases} v_{\mathrm{ini}}^{\mathrm{odd}}(\varepsilon\alpha) & \text{falls} \quad \alpha \text{ odd,} \\ v_{\mathrm{ini}}^{\mathrm{even}}(\varepsilon\alpha) & \text{falls} \quad \alpha \text{ even.} \end{cases} \tag{38}$$

In the case of periodic boundary conditions, the functions $r^{\,\mathrm{odd}}$, $r^{\,\mathrm{even}}$, $v^{\,\mathrm{odd}}$ and $v^{\,\mathrm{even}}$ are 1-periodic, whereas for Riemann problems all these function have a jump discontinuity within the interval $(0,\,1)$. Note that the initial data (37) are cold, if and only if $r^{\,\mathrm{odd}} = r^{\,\mathrm{even}}$ and $v^{\,\mathrm{odd}} = v^{\,\mathrm{even}}$.

We mention, that the class of modulated binary oscillation is not stable under the evolution. In other words, even if we start with unmodulated wave numbers we find non-constant wave numbers for all times $\overline{t} > 0$.

For all simulations we solve NEWTON's equations (2) with the VERLET-method (33) within a given macroscopic time interval $[0,\,\overline{t}_{\mathrm{end}}]$. Since we always use a constant time step size Δt, the number of time steps is proportional to the particle number. We choose Δt small in comparison to the smallest inverse frequency t_{lin} of the linearized problem. The value of t_{lin} can be approximated by the period t_{BO} of the linearized binary oscillator, i.e.

$$t_{\mathrm{lin}} \;\approx\; t_{\mathrm{BO}} \;=\; \frac{2\pi}{\sqrt{\Phi''(\overline{r})}}. \tag{39}$$

Here $\overline{r}$ denotes the local mean value of the atomic distances, and can be estimated during the computation. In all simulation we have ensured that there hold $\Delta t/t_{\mathrm{BO}} \lessapprox 0.01$ during the whole computation.

Windows in space-time

In order to study the macroscopic behavior of the atomic chain for large N we shall pass from the enormous amount of microscopic data to the characteristic macroscopic quantities, which are

1. the macroscopic fields of the local mean values, and
2. local distribution functions of the atomic data.

The main tool for computing the macroscopic data are space-time *windows* which are very small on the macroscopic scale, but which contain a lot of particles as well as time steps. In the sequel let $\mathcal{F}$ be a window, i.e.

$$\mathcal{F} \;=\; I_{\mathrm{T}}^{\mathcal{F}} \times I_{\mathrm{P}}^{\mathcal{F}}, \tag{40}$$

where $I_{\mathrm{T}}^{\mathcal{F}}$ and $I_{\mathrm{P}}^{\mathcal{F}}$ are sets of time steps and particle indices, respectively. $I_{\mathrm{T}}^{\mathcal{F}}$ and $I_{\mathrm{P}}^{\mathcal{F}}$ read

$$I_{\mathrm{T}}^{\mathcal{F}} \;=\; \Big\{i^{\mathcal{F}} - A_{\mathrm{T}}^{\mathcal{F}} + 1,\, ...,\, i^{\mathcal{F}} - 1,\, i^{\mathcal{F}}\Big\}, \tag{41}$$

$$I_{\mathrm{P}}^{\mathcal{F}} \;=\; \Big\{\alpha^{\mathcal{F}} - A_{\mathrm{P}}^{\mathcal{F}},\, ...,\, \alpha^{\mathcal{F}} - 1,\, \alpha^{\mathcal{F}},\, \alpha^{\mathcal{F}} + 1,\, ...,\, \alpha^{\mathcal{F}} + A_{\mathrm{P}}^{\mathcal{F}}\Big\}. \tag{42}$$

where $i^{\mathcal{F}}$ is a time steps, $\alpha^{\mathcal{F}}$ is a particle index, and $A_{\mathrm{P}}^{\mathcal{F}}$, $A_{\mathrm{T}}^{\mathcal{F}}$ are two integers satisfying

$$1 \ll A_{\mathrm{P}}^{\mathcal{F}},\, A_{\mathrm{T}}^{\mathcal{F}} \ll N. \tag{43}$$

If $t^{\mathcal{F}}$ denotes the microscopic time corresponding to $i^{\mathcal{F}}$, the window $\mathcal{F}$ contains all microscopic data around the macroscopic point $Z^{\mathcal{F}}$, where

$$Z^{\mathcal{F}} \;=\; \big(\varepsilon t^{\mathcal{F}},\, \varepsilon\alpha^{\mathcal{F}}\big). \tag{44}$$

For any atomic observable ψ we can now compute the mean value $\langle\psi\rangle_{\mathcal{F}}$ of ψ with respect two $\mathcal{F}$. If ψ is a one-particle observables there immediately results

$$\langle\psi\rangle_{\mathcal{F}} \;=\; \frac{1}{A_{\mathrm{T}}^{\mathcal{F}}(2A_{\mathrm{P}}^{\mathcal{F}} + 1)} \sum_{(i,\,\alpha)\in\mathcal{F}} \psi\big(r_{\alpha}^{(i)},\, v_{\alpha}^{(i)}\big), \tag{45}$$

and if the values von ψ depend on the data of more than one particle, similar formulas for $\langle\psi\rangle_{\mathcal{F}}$ may be easily derived.

Next we describe how we compute the distribution functions of the atomic data within a window $\mathcal{F}$. We consider solely the distribution functions in the microscopic phase phase, that we have introduced in Section 2 as the plane spanned by atomic distance and atomic velocity. For any window $\mathcal{F}$ we choose a rectangle $B^{\mathcal{F}}$ in the microscopic phase space

$$B^{\mathcal{F}} \;=\; \Big\{(r,\, v) \;:\; r_{\mathrm{min}}^{\mathcal{F}} < r \le r_{\mathrm{max}}^{\mathcal{F}}, \quad v_{\mathrm{min}}^{\mathcal{F}} < v \le v_{\mathrm{max}}^{\mathcal{F}}\Big\}, \tag{46}$$

and decompose it into $M_{\mathrm{r}}^{\mathcal{F}} \times M_{\mathrm{v}}^{\mathcal{F}}$ equal and pairwise disjunct sub-rectangles

$$B^{\mathcal{F}} \;=\; \bigcup_{m_{\mathrm{r}}=1..M_{\mathrm{r}}^{\mathcal{F}},\, m_{\mathrm{v}}=1..M_{\mathrm{v}}^{\mathcal{F}}} B_{m_{\mathrm{r}},\, m_{\mathrm{v}}}^{\mathcal{F}}, \tag{47}$$

`N`	:	number of particles N,
`ma_final_time`	:	macroscopic final time $\overline{t}_{\mathrm{end}}$,
`mi_final_time`	:	microscopic final time $t_{\mathrm{end}} = N\overline{t}_{\mathrm{end}}$,
`mi_time_delta`	:	length of microscopic time steps Δt,
`mi_time_steps`	:	number of microscopic time steps,
`mv_win_t_len`	:	parameter $A_{\mathrm{T}}^{\mathcal{F}}$ for MV-windows,
`mv_win_p_len`	:	value of $2A_{\mathrm{P}}^{\mathcal{F}}+1$ for MV-windows,
`df_win_t_len`	:	parameter $A_{\mathrm{T}}^{\mathcal{F}}$ for DF-windows,
`df_win_p_len`	:	value of $2A_{\mathrm{P}}^{\mathcal{F}}+1$ for DF-windows,
`df_win_prm`	:	parameter $M_{\mathrm{r}}^{\mathcal{F}} = M_{\mathrm{v}}^{\mathcal{F}}$ for DF-windows.

Table 1: Meaning of the numerical parameters. $\diamond$

where $M_{\mathrm{r}}^{\mathcal{F}}$ and $M_{\mathrm{v}}^{\mathcal{F}}$ are two integers controlling the resolution. We approximate the atomic distribution function within $\mathcal{F}$ by a $M_{\mathrm{r}}^{\mathcal{F}} \times M_{\mathrm{v}}^{\mathcal{F}}$-matrix $W^{\mathcal{F}}$, whose components $W_{m_{\mathrm{r}},m_{\mathrm{v}}}^{\mathcal{F}}$ are given by

$$W_{m_{\mathrm{r}},m_{\mathrm{v}}}^{\mathcal{F}} = \mu^{\mathcal{F}}\,\sharp\Big\{(i,\,\alpha)\in\mathcal{F}\,:\,\big(r_{\alpha}^{(i)},\,v_{\alpha}^{(i)}\big)\in B_{m_{\mathrm{r}},m_{\mathrm{v}}}^{\mathcal{F}}\Big\}. \tag{48}$$

Here $\sharp$ means the number of elements, and $\mu^{\mathcal{F}}$ is a normalization constant. It is obvious, that the Matrix $W^{\mathcal{F}}$ approximates the distribution function of the atomic data only if the rectangle $B^{\mathcal{F}}$ is sufficiently large. In particular, for all $(i,\,\alpha)\in\mathcal{F}$ the point $(r_{\alpha}^{(i)},\,v_{\alpha}^{(i)})$ should be an element of $B^{\mathcal{F}}$. For this reason we shall determine the bounds of $B^{\mathcal{F}}$ not a-priori, but during the numerical computation.

For practical purposes it is convenient to distinguish between two kinds of space-time windows - *MV-windows* to compute the means values, and *DF-windows* for the evaluation of distribution functions. MV-windows should be rather large, in order to prevent oscillations in the mean values. On the other hand, DV-windows should be rather small, so that the fine structure of the microscopic oscillations become as clear as possible.

The traveling wave within a window

The micro-macro transition from Section 2 relies on the hypothesis, that all oscillations of the atomic data can be described in terms of modulated traveling waves. Here we describe, how we can check this hypothesis in our numerical simulations. As in the previous section, we use space-time windows, which again are small on the macroscopic scale, but very large in microscopic units.

If the atomic oscillations are equivalent to those from modulated traveling waves, the microscopic distributions functions within any space-time window $\mathcal{F}$ must be equivalent to the distribution function of an exact traveling wave. Of course, the parameters of this exact traveling wave may depend on the window $\mathcal{F}$.

As discussed in Section 2, for any $\mathcal{F}$ we have to identify four traveling wave parameters, namely the specific length $r_{\mathcal{F}}$, die mean velocity $v_{\mathcal{F}}$, the wave number $k_{\mathcal{F}}$ and a fourth parameter, which might be either the frequency $\omega_{\mathcal{F}}$, the parameter $\gamma_{\mathcal{F}}$, the entropy $S_{\mathcal{F}}$, or the temperature $T_{\mathcal{F}}$.

The values of the specific length and of the mean velocity are fixed by their physical meaning: $r_{\mathcal{F}}$ and $v_{\mathcal{F}}$ result as the local mean values of the atomic distances and velocities, respectively, i.e. we set

$$r_{\mathcal{F}} := \langle r \rangle_{\mathcal{F}}, \qquad v_{\mathcal{F}} := \langle v \rangle_{\mathcal{F}}. \tag{49}$$

Similarly, the temperature $T_{\mathcal{F}}$ is computed as the twofold mean internal kinetic energy, which reads

$$T_{\mathcal{F}} := \left\langle (v - \langle v \rangle_{\mathcal{F}})^2 \right\rangle_{\mathcal{F}} = \left\langle v^2 \right\rangle_{\mathcal{F}} - \langle v \rangle_{\mathcal{F}}^{\;2}. \tag{50}$$

The determination of wave number $k_{\mathcal{F}}$ and frequency $\omega_{\mathcal{F}}$ is not so obvious, because they have no immediate physical interpretation on the microscopic scale. For this reason we introduce *auxiliary observables* Ψ_k and Ψ_ω, and set

$$k_{\mathcal{F}} := \langle \Psi_k \rangle_{\mathcal{F}}, \qquad \omega_{\mathcal{F}} := \langle \Psi_\omega \rangle_{\mathcal{F}}. \tag{51}$$

The auxiliary variables in our simulations are given by

$$(\Psi_k)_\alpha^{(i)} := \frac{\operatorname{ang}\left(P_{\alpha-1}^{(i)},\, P_\alpha^{(i)}\right)}{2\pi} \mod 1, \tag{52}$$

$$(\Psi_\omega)_\alpha^{(i)} := \left| \frac{\operatorname{ang}\left(P_\alpha^{(i-1)},\, P_\alpha^{(i)}\right)}{2\pi\Delta t} \right|, \tag{53}$$

where

$$P_\alpha^{(i)} = Q_{\alpha+1}^{(i)} - Q_\alpha^{(i)} \quad \text{with} \quad Q_\alpha^{(i)} = \left(r_\alpha^{(i)},\, v_\alpha^{(i)}\right),$$

and $\operatorname{ang}(P_1,\, P_2)$ denotes the angle between the vectors $P_1 = (r_1,\, v_1)^T$ and $P_2 = (r_2,\, v_2)^T$, i.e.

$$\operatorname{ang}(P_1,\, P_2) = \operatorname{sgn}(+r_1 v_2 - r_2 v_1) \arccos\left(\frac{r_1 r_2 + v_1 v_2}{|P_1|\,|P_2|}\right).$$

Note that Ψ_k takes values in $[0, 1]$, and that Ψ_ω is non-negative. The formulas (51)–(53) were tested with exact traveling wave solutions, for which they reproduce the right values for $k_{\mathcal{F}}$ and $\omega_{\mathcal{F}}$. Finally, we define $S_{\mathcal{F}}$ consistent to Section 2 by $S_{\mathcal{F}} := T_{\mathcal{F}}/\omega_{\mathcal{F}}$. In the next step we use the values $r_{\mathcal{F}}$, $v_{\mathcal{F}}$, $k_{\mathcal{F}}$ and $T_{\mathcal{F}}$ in order to associate to any window F an exact traveling wave with these parameters. For that purpose we use an approximation scheme for traveling waves as it is described in [DH05][1]. This scheme provides

[1] To be more precise, we use the T-scheme from [DH05], which allow the prescription of the temperature.

Atomic observable	Definition
distance	$r_\alpha(t) = x_{\alpha+1}(t) - x_\alpha(t)$
velocity	$v_\alpha(t) = \dot{x}_\alpha(t)$
negative force	$p_\alpha(t) = -\Phi'(r_\alpha(t))$
energy	$e_\alpha(t) = \frac{1}{2}(v_{\alpha+1}(t))^2 + \Phi(r_\alpha(t))$
energy flux	$f_\alpha(t) = -v_\alpha(t)\,\Phi'(r_\alpha(t))$

Table 2: Selected atomic observables.⋄

	mean value	**TW-mean value**
specific length	$r_\mathcal{F} = \langle\text{distance}\rangle_\mathcal{F}$	$r_\mathcal{F}^\text{TW} = \langle\text{distance}\rangle_\mathcal{F}^\text{TW}$
macroscopic velocity	$v_\mathcal{F} = \langle\text{velocity}\rangle_\mathcal{F}$	$v_\mathcal{F}^\text{TW} = \langle\text{velocity}\rangle_\mathcal{F}^\text{TW}$
pressure	$p_\mathcal{F} = \langle\text{neg. force}\rangle_\mathcal{F}$	$p_\mathcal{F}^\text{TW} = \langle\text{neg. force}\rangle_\mathcal{F}^\text{TW}$
macroscopic energy density	$e_\mathcal{F} = \langle\text{energy}\rangle_\mathcal{F}$	$e_\mathcal{F}^\text{TW} = \langle\text{energy}\rangle_\mathcal{F}^\text{TW}$
macroscopic energy flux	$f_\mathcal{F} = \langle\text{energy flux}\rangle_\mathcal{F}$	$f_\mathcal{F}^\text{TW} = \langle\text{energy flux}\rangle_\mathcal{F}^\text{TW}$
	field	**TW-field**
frequency	$\omega_\mathcal{F}$ is mean value	$\omega_\mathcal{F}^\text{TW}$ from T-Scheme
entropy	$S_\mathcal{F} = T_\mathcal{F}/\omega_\mathcal{F}$	$S_\mathcal{F}^\text{TW} = T_\mathcal{F}^\text{TW}/\omega_\mathcal{F}^\text{TW}$
heat flux	$q_\mathcal{F} = f_\mathcal{F} - p_\mathcal{F}\,v_\mathcal{F}$	$q_\mathcal{F}^\text{TW} = f_\mathcal{F} - p_\mathcal{F}^\text{TW}\,v_\mathcal{F}^\text{TW}$
entropy flux	$g_\mathcal{F} = q_\mathcal{F}/\omega_\mathcal{F}$	$g_\mathcal{F}^\text{TW} = q_\mathcal{F}^\text{TW}/\omega_\mathcal{F}^\text{TW}$

Table 3: Mean values and derived fields.⋄

1. two profile functions $\mathbb{R}_\mathcal{F}$ and $\mathbb{V}_\mathcal{F}$, which give the atomic distances and velocities, respectively, of the exact traveling wave,
2. a frequency $\omega_\mathcal{F}^\text{TW}$, which does not result from the auxiliary observable (53), but satisfies a dispersion relation.

Employing $\omega_\mathcal{F}^\text{TW}$ and the profile functions $\mathbb{R}_\mathcal{F}$ and $\mathbb{V}_\mathcal{F}$ we can

1. derive the corresponding distribution function in the microscopic phase space,
2. define an entropy $S_\mathcal{F}^\text{TW}$ by $S_\mathcal{F}^\text{TW} = S_\mathcal{F}^\text{TW}/\omega_\mathcal{F}^\text{TW}$,

3. compute for any observable ψ a corresponding *TW-mean value* $\langle\psi\rangle_{\mathcal{F}}^{\mathrm{TW}}$. For instance, for the pressure $p_{\mathcal{F}}^{\mathrm{TW}}$ there results

$$p_{\mathcal{F}}^{\mathrm{TW}} = -\int_0^1 \Phi'(r_{\mathcal{F}} + \mathbb{R}_{\mathcal{F}}(\varphi + k_{\mathcal{F}}/2))\,\mathrm{d}\varphi. \tag{54}$$

Since we use $r_{\mathcal{F}}$, $v_{\mathcal{F}}$, $k_{\mathcal{F}}$ and $T_{\mathcal{F}}$ to determine an exact traveling wave, the following identities are satisfied by construction

$$r_{\mathcal{F}}^{\mathrm{TW}} = r_{\mathcal{F}}, \quad v_{\mathcal{F}}^{\mathrm{TW}} = v_{\mathcal{F}}, \quad k_{\mathcal{F}}^{\mathrm{TW}} = k_{\mathcal{F}} \quad \text{and} \quad T_{\mathcal{F}}^{\mathrm{TW}} = T_{\mathcal{F}}. \tag{55}$$

However, it is not ensured by our definitions that there hold $\omega_{\mathcal{F}} = \omega_{\mathcal{F}}^{\mathrm{TW}}$, $S_{\mathcal{F}} = S_{\mathcal{F}}^{\mathrm{TW}}$, or $\langle\psi\rangle_{\mathcal{F}} = \langle\psi\rangle_{\mathcal{F}}^{\mathrm{TW}}$ for all observables ψ. The validity of these identities have to be checked!

In Table 2 we have summarized the most important atomic observables. The corresponding mean values and further derived quantities are described in Table 3.

From now on we call the distribution functions, which result directly from the atomic data, the *microscopic distribution functions*. Since the traveling wave parameters $r_{\mathcal{F}}$, $v_{\mathcal{F}}$, $k_{\mathcal{F}}$, and $T_{\mathcal{F}}$ vary only on the macroscopic scale, we call the distribution functions, which result from the profile functions $\mathbb{R}_{\mathcal{F}}$ and $\mathbb{V}_{\mathcal{F}}$, the *macroscopic predictions*. Moreover, to distinguish between the different notions of mean values, we refer to $\langle\psi\rangle_{\mathcal{F}}$ and $\langle\psi\rangle_{\mathcal{F}}^{\mathrm{TW}}$ as *fields* and *TW-fields*, respectively.

Since for any macroscopic point $P = (\overline{t}, \overline{\alpha})$ there is a space-time window $\mathcal{F}_P$ around P, i.e. $P = Z^{\mathcal{F}_P}$, we are allowed to interpret all macroscopic fields as well as all TW-fields as functions which depend on $\overline{t}$ and $\overline{\alpha}$.

We summarize this section: In order to check the hypothesis about the atomic oscillations in the numerical simulations, we shall compare

1. microscopic distribution functions with their macroscopic predictions,

2. various fields with their corresponding TW-fields.

The microscopic oscillations can be described in terms of modulated traveling waves, if and only if all comparisons yield a positive result.

3.2 Smooth data

The results of the numerical simulations will be presented graphically. As in section 2, we always plot the atomic data as well as the macroscopic fields against the macroscopic particle index $\overline{\alpha} \in [0, 1]$ for fixed macroscopic time $\overline{t}$. Moreover, the microscopic distribution functions are always presented as density plots.

N	=	2000/4000			
ma_final_time	=	5.0E-01	mi_final_time	=	1.0E+03 /2.0E+03
mi_time_delta	=	1.0E-02	mi_time_steps	=	100000 /200000
mv_win_t_len	=	3577/5059	mv_win_p_len	=	5/10
df_win_t_len	=	3577/5059	df_win_p_len	=	10/20
df_win_prm	=	100			

Table 4: Numerical parameters for Example $S1$. $\diamond$

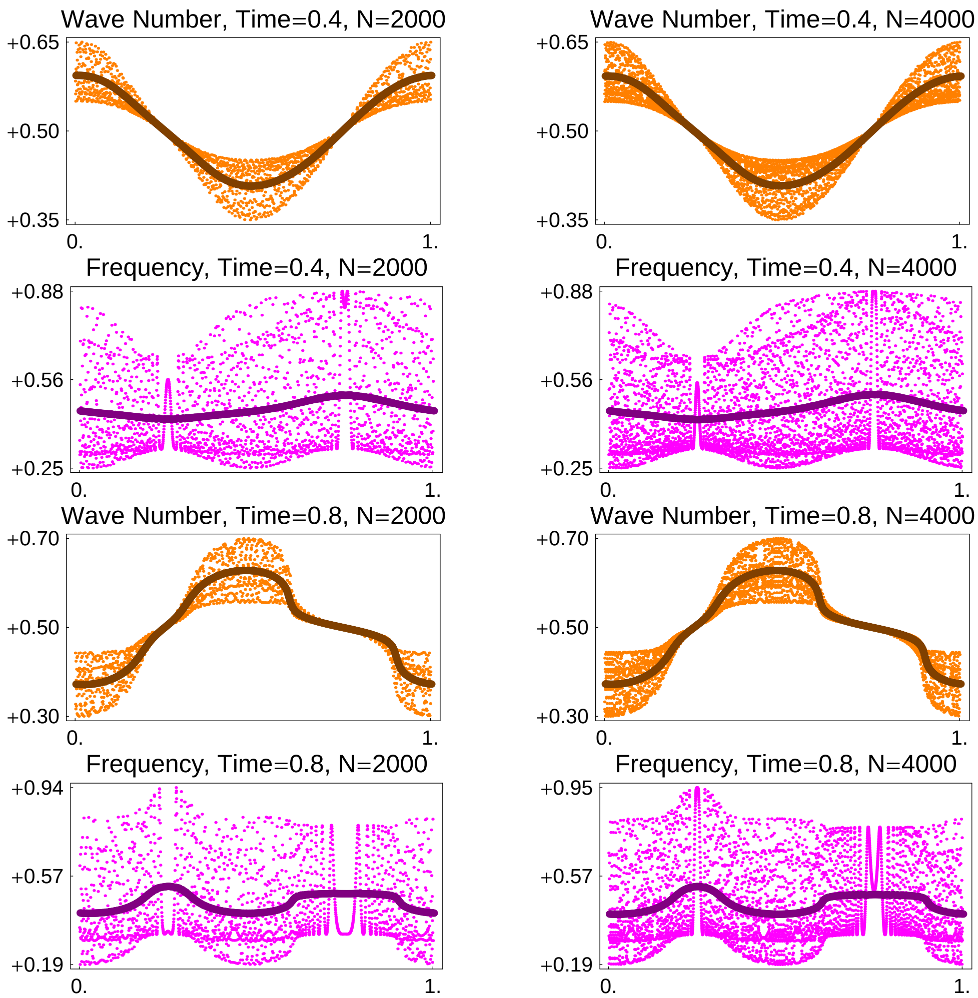

Figure 9: Computation of wave number and frequency for Example $S1$. We see the oscillating values of the auxiliary observables as well as their macroscopic mean values. The left and right column correspond to $N = 2000$ and $N = 4000$, respectively. $\diamond$

Example $S1$

We return to the second Example from Section 2. In particular, the initial data for Example $S1$ are given by Equation (16) and Figure 5 from Section 2. Note that at

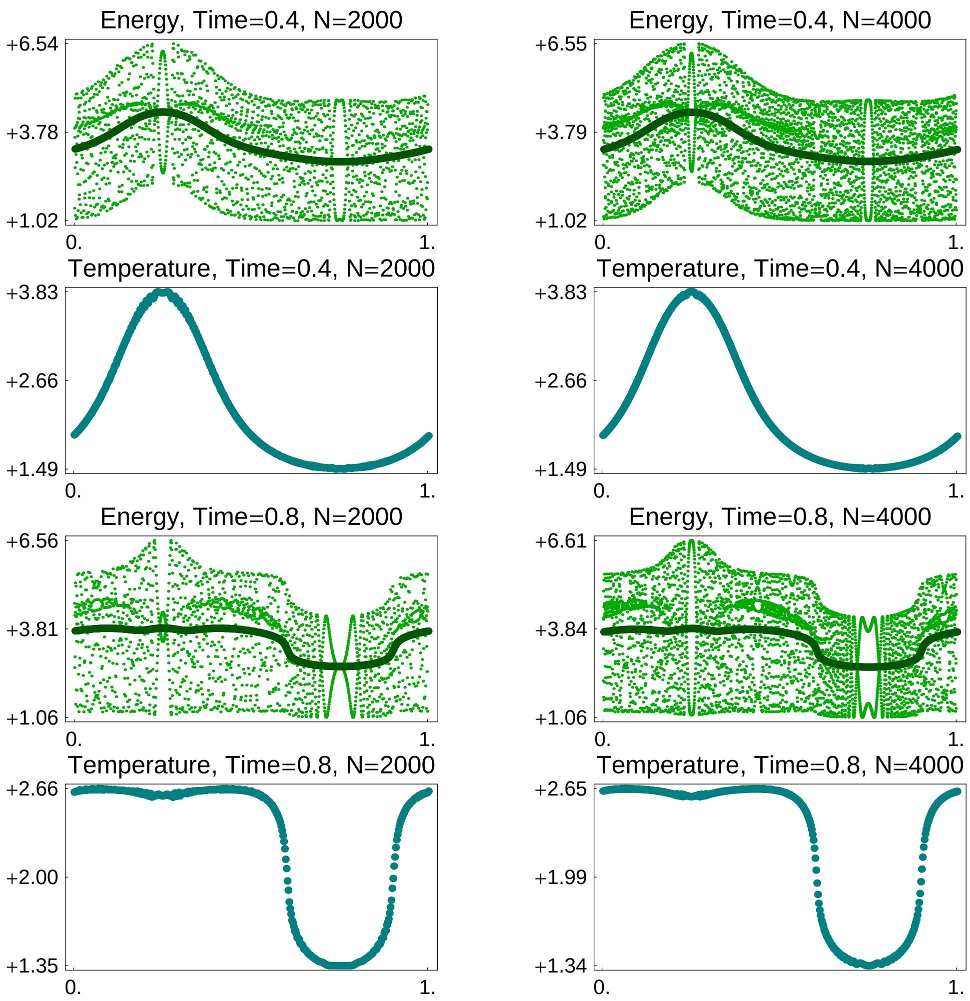

Figure 10: Atomic energy E and macroscopic temperature T for Example $S1$. $\diamond$

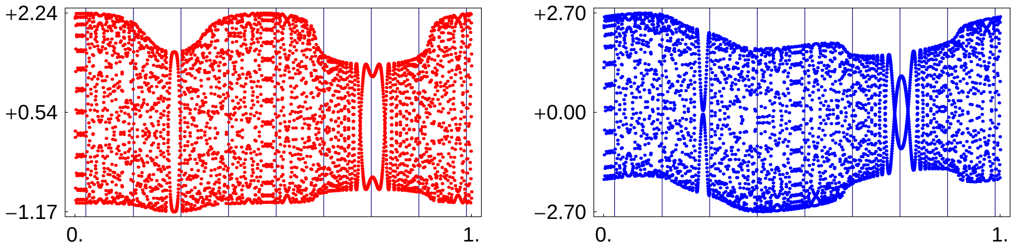

Figure 11: The vertical lines mark the $\overline{\alpha}$-coordinate of the macroscopic points, where we evaluate the microscopic distribution functions in Figure 12. There holds $\overline{t} = 0.8$. $\diamond$

$\overline{t} = 0$ we modulate only the macroscopic velocity v, but neither the specific length r, nor the wave number k or the internal energy U.

The atomic distances and velocities for $\overline{t} > 0$ are presented in Figures 6 and 7, and Figure 10 shows the oscillating atomic energy, their macroscopic mean value, and

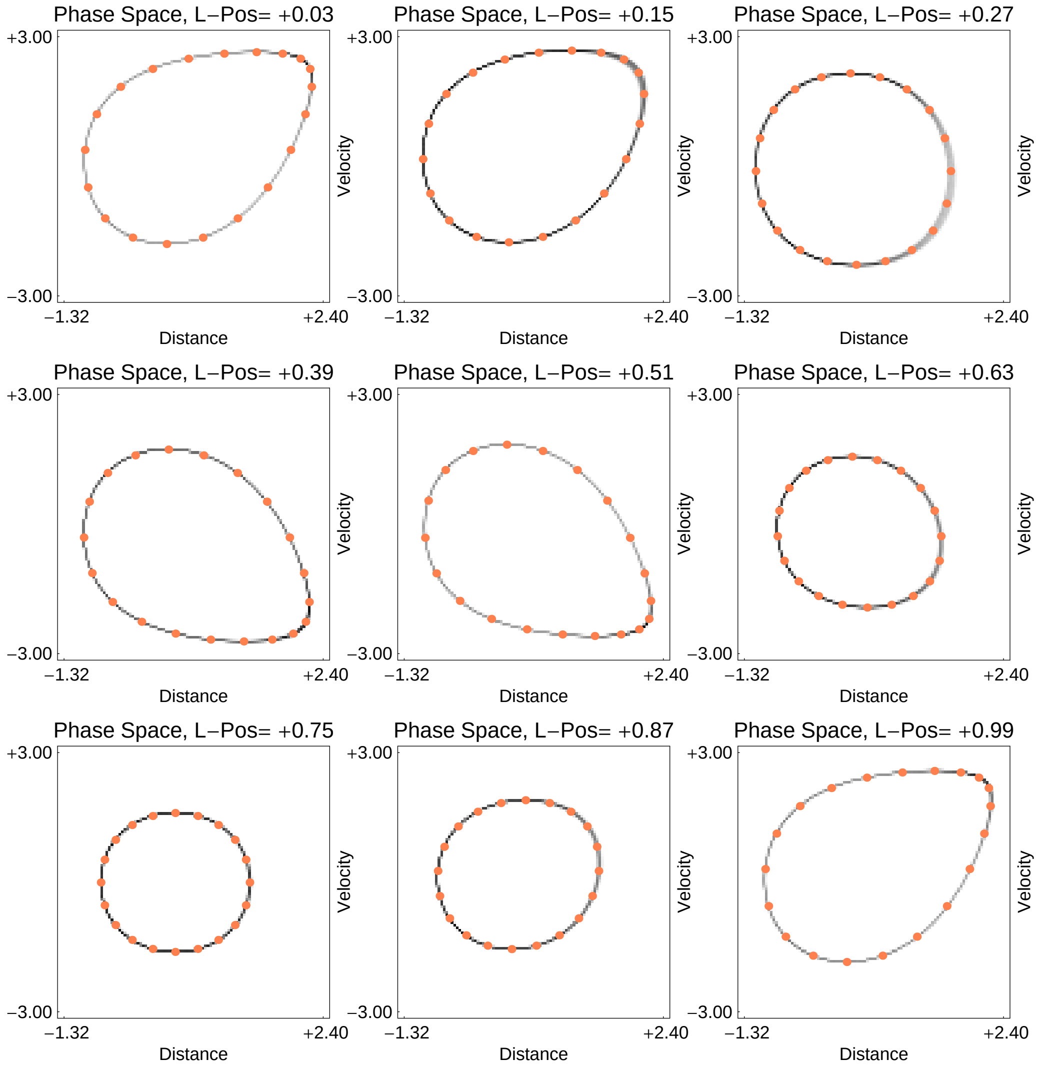

Figure 12: Local distribution functions for Example $S1$ with $N = 4000$ corresponding to the nine macroscopic points from Figure 11. Gray and Orange correspond to microscopic distribution functions and macroscopic predictions, respectively. $\diamond$

the macroscopic temperature.

The computation of wave number and frequency is illustrated in Figure 9. We see for different times ($\bar{t} = 0.4$ and $\bar{t} = 0.8$) and for different particle numbers ($N = 2000$ and $N = 4000$) the values of the auxiliary observables Ψ_k and Ψ_Ω. Again we observe high oscillations in the atomic data, which converge for $N \to \infty$ to a YOUNG-measure. However, the local mean values of the auxiliary observables converge to macroscopic functions, which give the fields of wave number and the frequency.

In the next step we compare the microscopic distribution functions with their macroscopic predictions in nine selected macroscopic points. These nine points are exactly

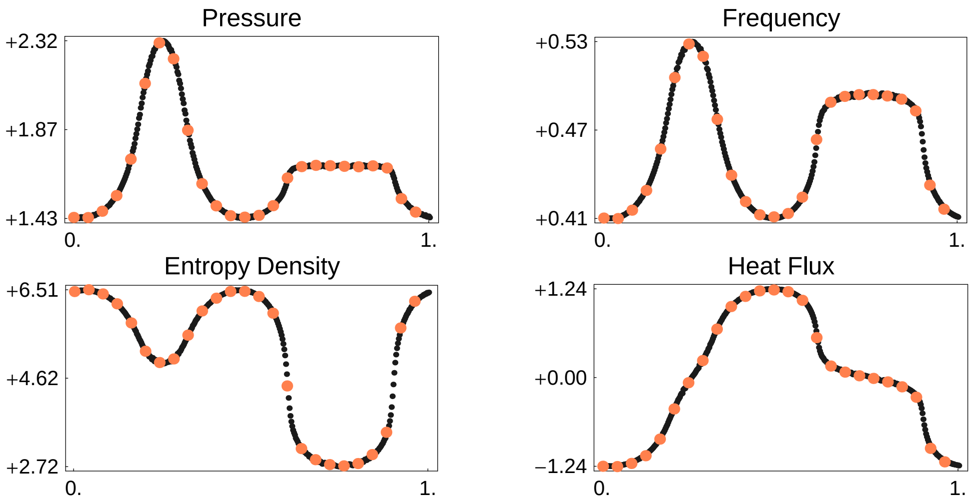

Figure 13: Comparison between macroscopic fields (black) and corresponding TW-fields (orange). There hold $N = 4000$ and $\bar{t} = 0.8$. ⋄

the same as in Figure 8, and we have marked their positions by the vertical lines in Figure 11. The size of the underlying space-time windows can be read off from Table 4.

Figure 12 shows the density plots from Figure 8 together with some orange drawn dots, which correspond to the macroscopic predictions, and which are obtained as follows. Let a window $\mathcal{F}$ be fixed. The values $r_{\mathcal{F}}$, $v_{\mathcal{F}}$, $k_{\mathcal{F}}$ and $T_{\mathcal{F}}$ determine an exact traveling wave with profiles functions $\mathbb{R}_{\mathcal{F}}$ and $\mathbb{V}_{\mathcal{F}}$, see the previous subsection, and [DH05] for more details. Then we compute for twenty different values φ_i of the phase the corresponding points Q_i in the microscopic phase space, where

$$Q_i \quad = \quad \left(r_{\mathcal{F}} + \mathbb{R}_{\mathcal{F}}(\varphi_i + k_{\mathcal{F}}/2),\, v_{\mathcal{F}} + \omega_{\mathcal{F}}\mathbb{V}_{\mathcal{F}}(\varphi_i)\right) \tag{56}$$

and $\varphi_i = i/20$, $i = 1...20$. Finally, we have drawn the points Q_i with orange color into the density plots of the microscopic distribution functions.

The nine plots of Figure 12 reveal (i) that the curve (56) coincides with the support of the microscopic distribution functions, and (ii) that the distance between Q_{i+1} and Q_i is related to the gray level of the microscopic distribution functions. From this we conclude that microscopic distribution functions and macroscopic predictions are in fact the same. This implies that the macroscopic evolution of all fields is governed by the modulation equations (6).

Finnaly, in Figure 13 we compare some macroscopic fields with their corresponding TW-fields. Note that we have plotted the values of the TW-fields in only 25 points. Recall that the definitions of the various fields and TW-fields are given in Table 3. In particular, all fields result immediately from the atomic data, whereas all TW-fields depend only on the four macroscopic fields r^{TW}, v^{TW}, k^{TW} and T^{TW}. We observe a perfect correspondence between fields and TW-fields, which gives another confirmation for the validity of modulation theory.

The modulation equations for the harmonic chain, see Equation (32), split into two independent subsystems. The first one describes the evolution of the mechanical fields mass and momentum, whereas the second one is related to wave number and entropy. Consequently, if we would initialize the harmonic chain with the initial data 16, the wave number and the entropy would remain constant for all times. As the current example shows, in the nonlinear case there is in general a coupling between all four modulation equations.

Example $S2$

In this example we study the evolution of smooth initial data for an interaction potential, that is not integrable. To this end we add a term of fourth order to the TODA-potential, namely

$$\Phi(r) \quad = \quad \exp\left((1-r)\right) - (1-r) + \frac{1}{40}(r-1)^4. \tag{57}$$

The initial data are shown in Figure 14. There holds $v^{\,\mathrm{odd}}(\overline{\alpha}) = v^{\,\mathrm{even}}(\overline{\alpha}) = 0$ and

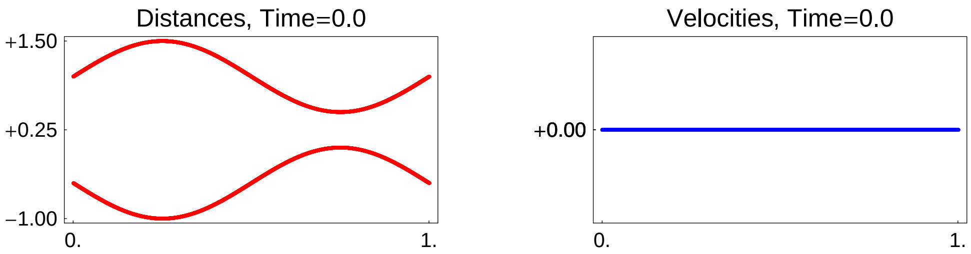

Figure 14: Modulated atomic initial data for Example $S2$. $\diamond$

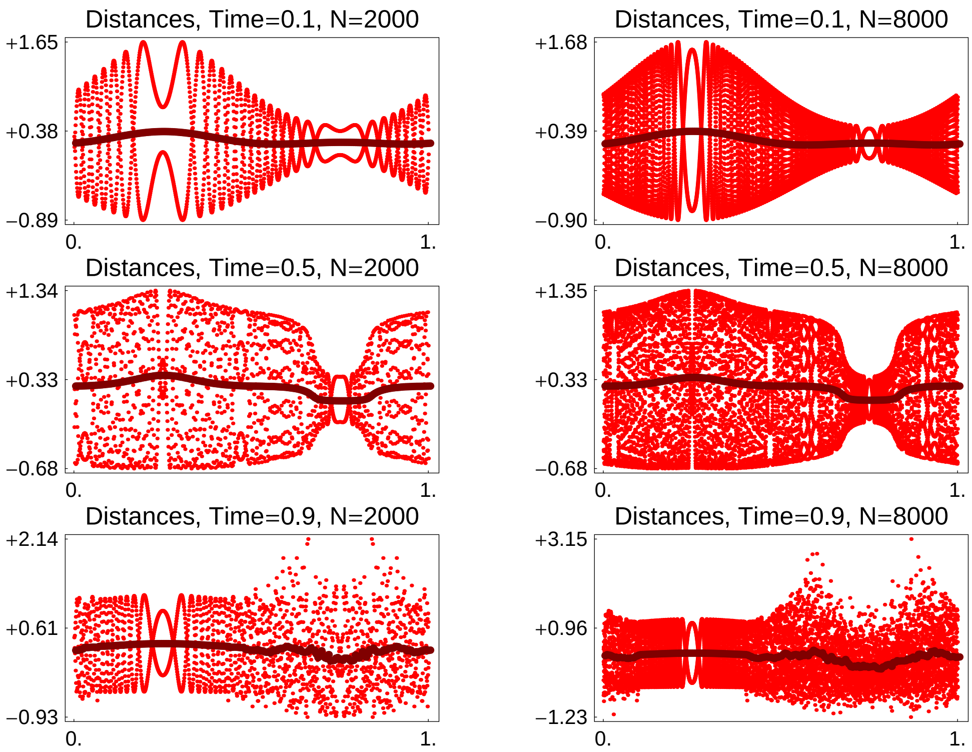

Figure 15: Evolution of the atomic distances for Example $S2$. The left and right column correspond to $N = 2000$ and $N = 8000$, respectively. The dark colored functions represent the local mean values. $\diamond$

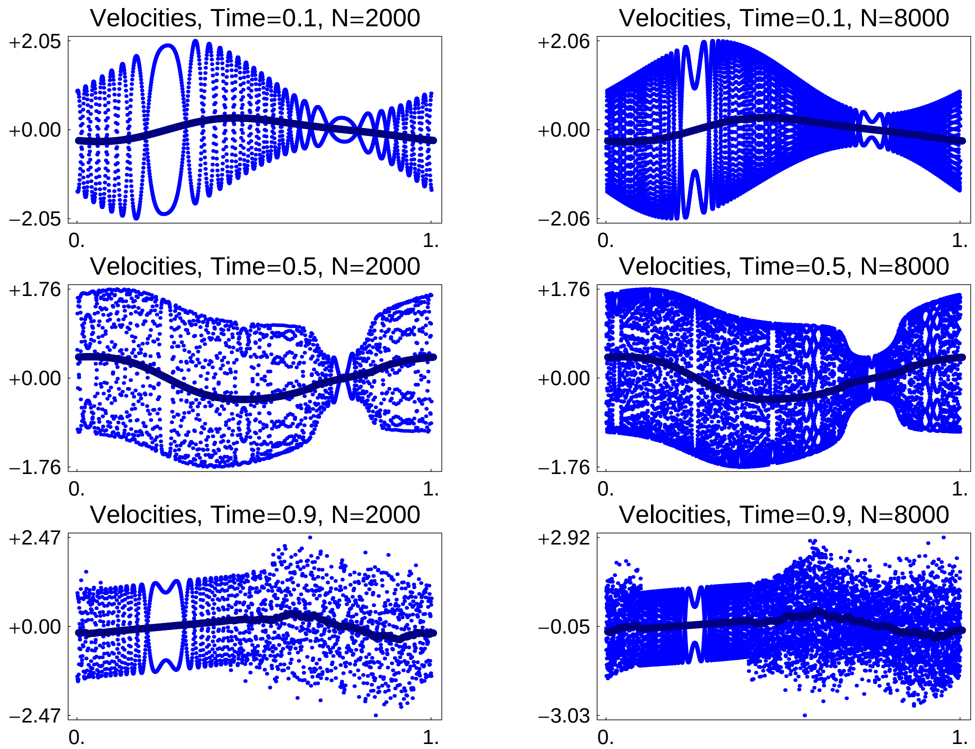

Figure 16: The atomic velocities to Figure 15. $\diamond$

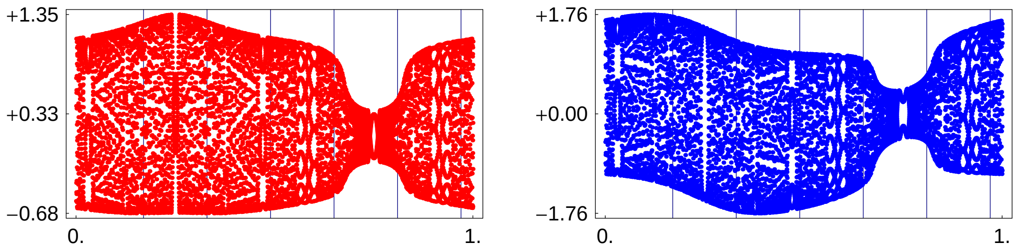

Figure 17: The vertical lines mark the $\overline{\alpha}$-coordinate of the macroscopic points, for which we evaluate the microscopic distribution functions in Figure 18. There holds $\overline{t} = 0.5$. $\diamond$

$$r^{\,\mathrm{odd}}(\overline{\alpha}) \;=\; 1 + \frac{1}{2}\sin(2\pi\overline{\alpha}), \qquad r^{\,\mathrm{even}}(\overline{\alpha}) \;=\; -\frac{1}{2} - \frac{1}{2}\sin(2\pi\overline{\alpha}).$$

Note the modulation of the internal energy U, which leads to a modulation of frequency ω and entropy S. However, the fields r, v and k are constant in the initial data. The solution of NEWTON's equation for different particle numbers ($N = 2000$ and $N = 8000$) and for various times ($\overline{t} = 0.1$, $\overline{t} = 0.5$, and $\overline{t} = 0.9$) is shown in Figures 15 and 16.

Until $\overline{t} \approx 0.5$ we observe the same qualitative behaviour as in Example $S1$: The atomic data converge for $N \to \infty$ to a YOUNG-measure, which implies that the local mean values converge in the sense of functions. Furthermore, the atomic oscillations are again bounded by sharp envelopes. In Figure 18 we compare the microscopic

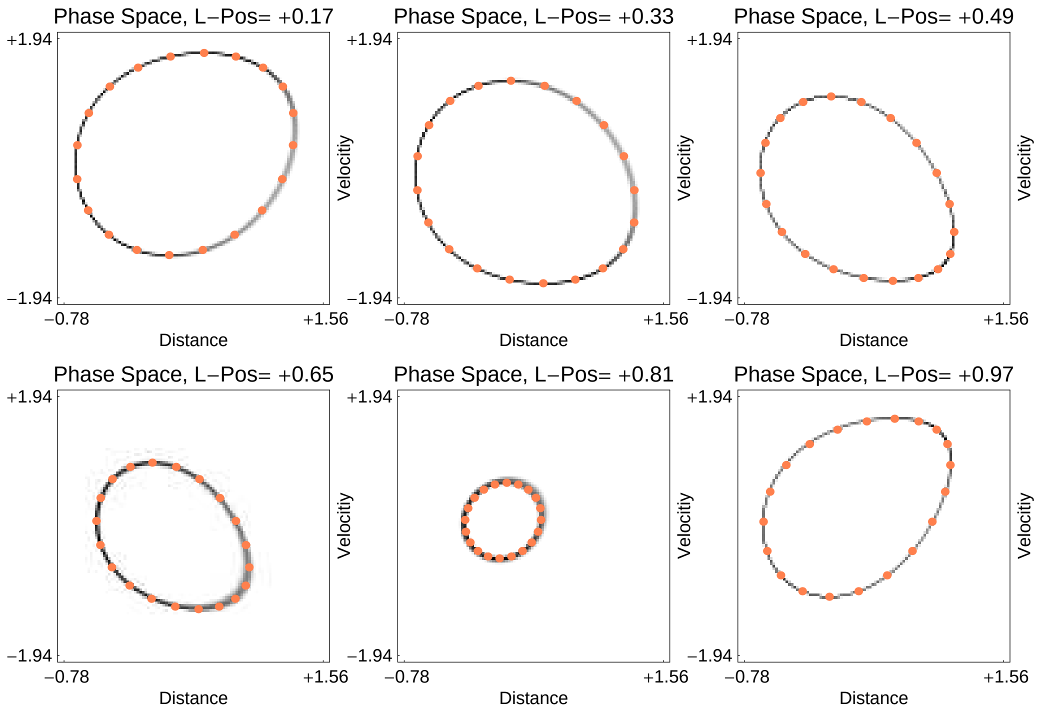

Figure 18: Local distribution functions in the microscopic phase space for Example $S2$ with $N = 8000$ and $\bar{t} = 0.5$, evaluated in the macroscopic points from Figure 17: Gray and Orange correspond to microscopic distributions and macroscopic predictions, respectively. **Interpretation**: Until $\bar{t} = 0.5$ all microscopic oscillations can be described by modulated traveling waves. ⋄

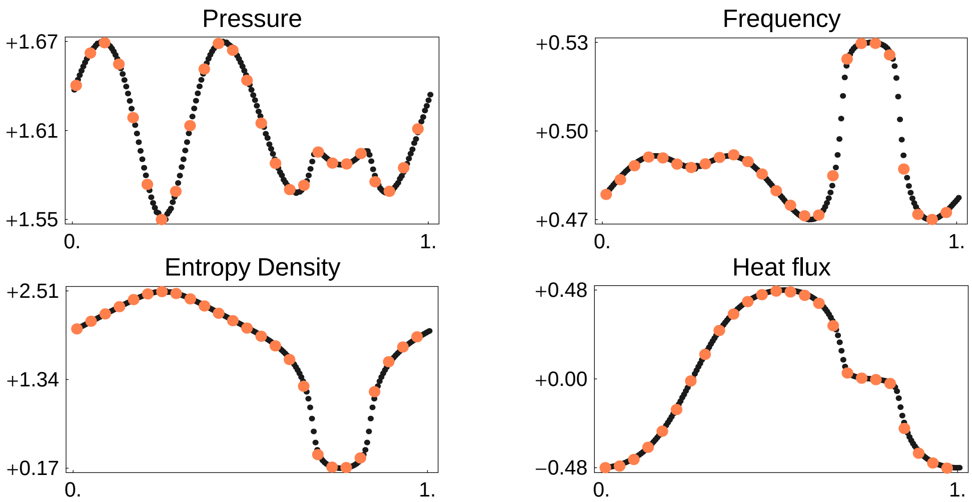

Figure 19: Comparison between macroscopic fields (black) and corresponding TW-fields (orange). There holds $N = 8000$ and $\bar{t} = 0.5$. ⋄

distribution functions with their macroscopic predictions in nine selected points at $\bar{t} = 0.5$, see Figure 17. We mention that we have used the same approach for this

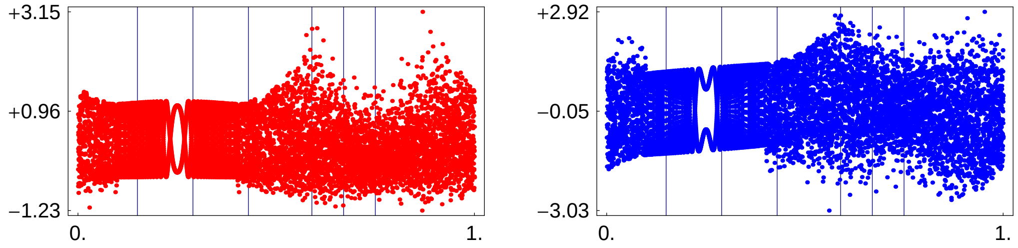

Figure 20: The vertical lines mark the $\overline{\alpha}$-coordinate of the macroscopic points, for which we evaluate the microscopic distribution functions in Figure 21. There holds $\overline{t} = 0.9$. $\diamond$

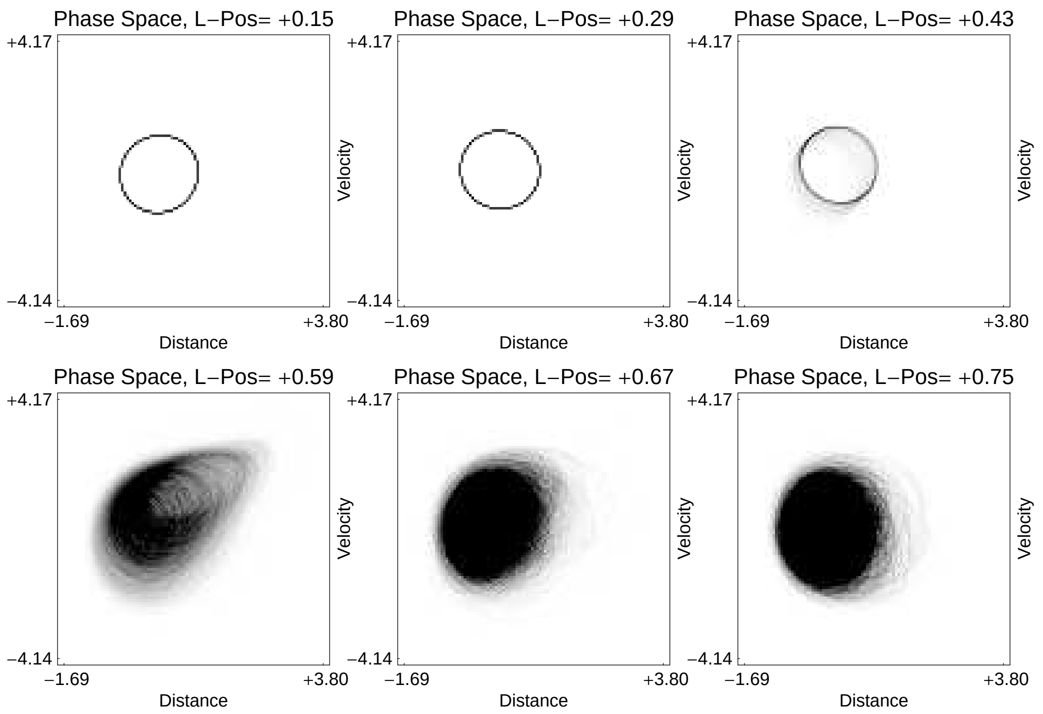

Figure 21: Local distribution functions in the microscopic phase space for Example $S2$ with $N = 8000$ and $\overline{t} = 0.9$, evaluated in the macroscopic points from Figure 20: Gray and Orange correspond to microscopic distributions and macroscopic predictions, respectively. **Interpretation**: After the formation of shocks, the microscopic oscillations exhibit a more complicated structure and can thus not longer be described by modulated traveling waves. $\diamond$

comparison as in the previous example, so that the orange drawn dots approximate the curve (56). As in Example $S1$, we observe a perfect correspondence between microscopic oscillations and macroscopic predictions. Similarly, Figure 19 yields the perfect matching of fields and TW-fields.

At $\overline{t} = 0.9$ we can identify a region, about $0.4 \lesssim \overline{\alpha} \lesssim 1.1$), where the microscopic oscillations exhibit a different behaviour. In Figure 21 we see that the support of

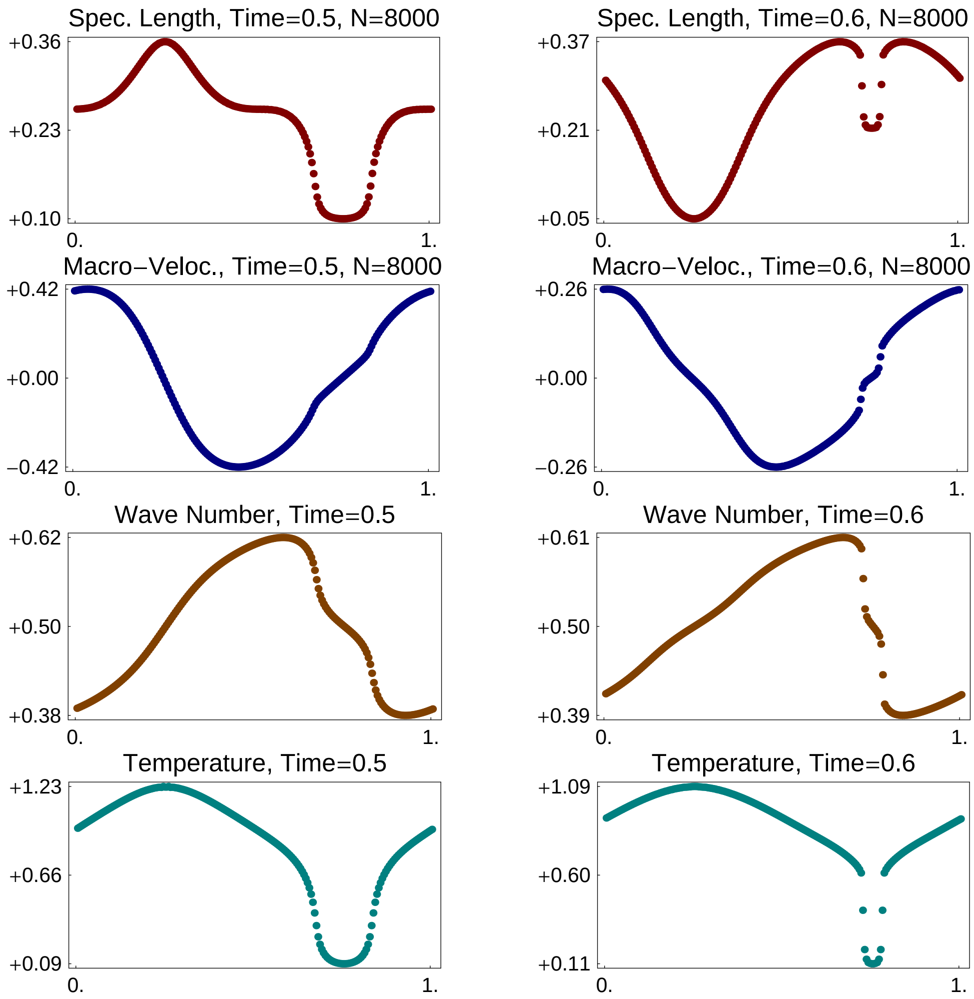

Figure 22: The formation of shocks in Example $S2$ with $N = 8000$. $\diamond$

N	=	2000/8000			
ma_final_time	=	0.9E+00	mi_final_time	=	1.8E+03 /7.2E+03
mi_time_delta	=	2.0E-02	mi_time_steps	=	90000 /360000
mv_win_t_len	=	2236/4472	mv_win_p_len	=	10/40
df_win_t_len	=	2236/4472	df_win_p_len	=	40/89
df_win_prm	=	100			

Table 5: Numerical parameters for Example $S2$. $\diamond$

the microscopic distribution functions are not longer contained in closed curves, but fill a set with positive measure. We conclude, that the microscopic oscillations in this region can not be described by modulated traveling waves.

Figure 22 provides an explanation for this phenomenon. We have plotted various macroscopic fields for $\bar{t} = 0.5$ and $\bar{t} = 0.6$. We observe that the gradients of all fields become steeper and steeper, so that finally there appear shocks, i.e. macroscopic discontinuities. These shocks are the reason, that modulated traveling waves fail to describe the microscopic oscillations. Consequently, the macroscopic evolution is not longer governed by the modulation equations (6). In what follows we will continue the investigation of macroscopic shocks.

Example $S3$

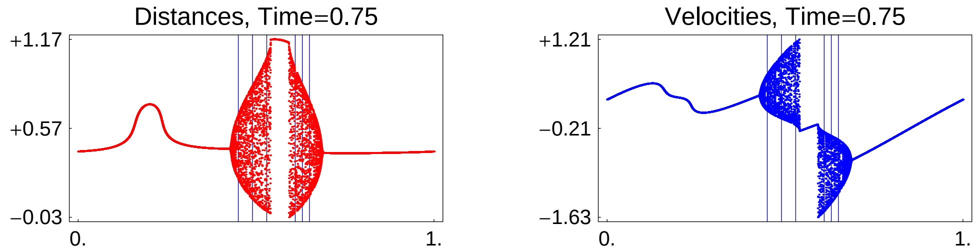

Figure 23: The atomic distances and velocities for Example $S3$ with $\overline{t} = 0.75$ and $N = 16000$. The vertical lines mark the $\overline{\alpha}$-coordinate of the macroscopic points, for which we evaluate the microscopic distribution functions in Figure 24. $\diamond$

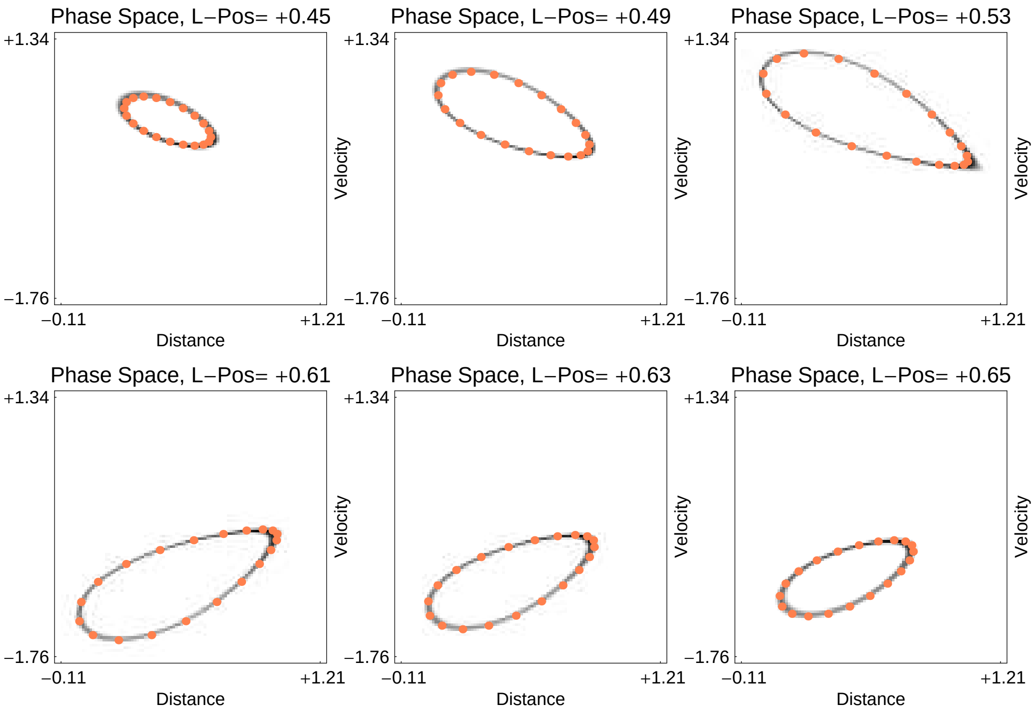

Figure 24: Local distribution functions for Example $S3$ with $N = 16000$ corresponding to the macroscopic points from Figure 23. Gray and Orange correspond to microscopic distribution functions and macroscopic predictions, respectively. **Interpretation**: Since the shocks result from cold data, the microscopic oscillations have the form of modulated traveling waves. $\diamond$

We revisit the first Example of Section 2, where we have considered modulated cold initial data that create temperature during the evolution, see Figures 3 and 4.

We study now the fine structure of the microscopic oscillations, which appear in the regions with temperature. To this end we compare in six selected points at $\overline{t} = 0.75$ the microscopic distribution functions with their macroscopic predictions, see Figure

N	=	16000			
ma_final_time	=	7.5E-01	mi_final_time	=	1.2E+04
mi_time_delta	=	1.0E-02	mi_time_steps	=	1200000
mv_win_t_len	=	9486	mv_win_p_len	=	80
df_win_t_len	=	9486	df_win_p_len	=	126
df_win_prm	=	100			

Table 6: Numerical parameters for Example $S3$. $\diamond$

23. The results are shown in Figure 24, and again we observe a perfect correspondence between microscopic distribution functions and macroscopic predictions. We conclude, that the modulation equations are able to describe macroscopic shocks which are generated by cold data, because these shocks lead to microscopic oscillations in form of modulated traveling waves. Recall the previous example, which has shown that the modulation equations may fail, if there appear shocks from data with temperature.

Example $S4$

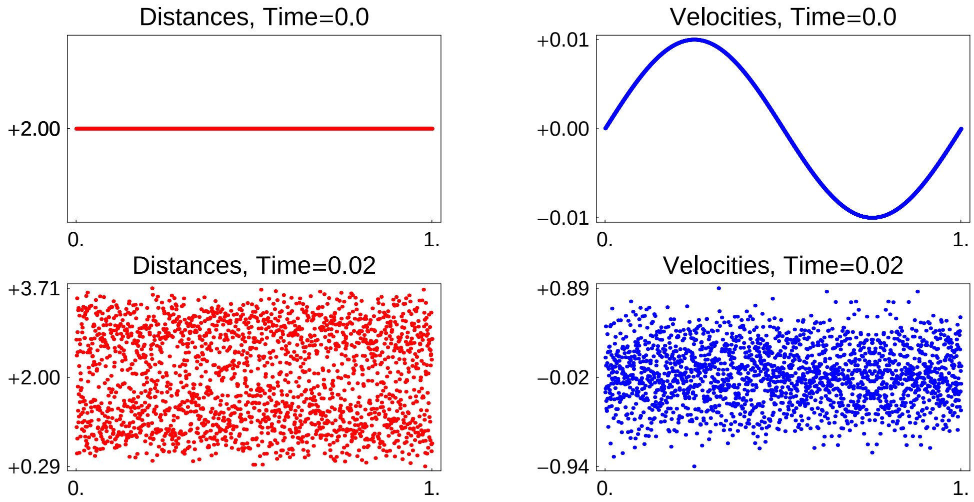

Figure 25: The atomic distances and velocities for Example $S4$ at times $\bar{t} = 0.0$ and $\bar{t} = 0.02$. ⋄

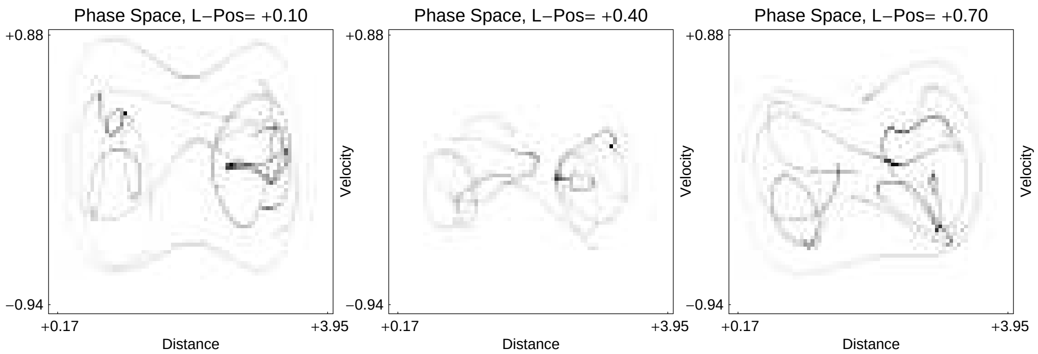

Figure 26: Local microscopic distribution functions for Example $S4$ in three selected points at $\bar{t} = 0.02$. **Interpretation**: Since Φ is non-convex, the microscopic oscillations can not be described by modulated traveling waves. ⋄

`N`	=	2000			
`ma_final_time`	=	2.0E-02	`mi_final_time`	=	4.0E+01
`mi_time_delta`	=	2.5E-03	`mi_time_steps`	=	16000
`df_win_t_len`	=	4000	`df_win_p_len`	=	5
`df_win_prm`	=	75			

Table 7: Numerical parameters for Example $S4$. ⋄

Up to now we have considered only convex interaction potentials. This restriction is essential, as the current example shows. We consider the following double-well potential

$$\Phi(r) = +2\cosh(2-r) - \sinh(1)(r-2)^2, \tag{58}$$

which has two stable equilibria at $r = 1$ and $r = 3$, and one unstable equilibrium at $r = 2$. Note that Φ is concave in the vicinity of $r = 2$. We initialize the chain with cold initial data,

$$r^{\,\mathrm{odd}}(\overline{\alpha}) \;=\; r^{\,\mathrm{even}}(\overline{\alpha}) \;=\; 2, \quad v^{\,\mathrm{odd}}(\overline{\alpha}) \;=\; v^{\,\mathrm{even}}(\overline{\alpha}) \;=\; \frac{1}{10}\cos\left(2\pi\overline{\alpha}\right),$$

and study the atomic evolution for small times $\overline{t} \lessapprox 0.02$, see Figure 25. Figure 26 contains the density plots of the resulting microscopic oscillations in three selected points at $\overline{t} = 0.02$. We observe that cold data produce immediately temperature in form of microscopic oscillations. However, these oscillations can not be described by modulated traveling waves, because they exhibit a completely different structure. In particular, the supports of the distribution functions are not contained in closed curves, which corresponds to the absence of sharp envelopes in Figure 25.

This result is not surprising, because for non-convex interaction potentials Φ, the system (28) is not hyperbolic (in the regions of concavity it is even elliptic).

3.3 RIEMANN problems

For the numerical solution of RIEMANN problems we use the following boundary conditions

$$x_0^{(i)} = x_1^{(i)} + x_2^{(i)} - x_3^{(i)} \quad \text{and} \quad x_{N+1}^{(i)} = x_N^{(i)} + x_{N-1}^{(i)} - x_{N-2}^{(i)}. \tag{59}$$

These boundary conditions are appropriate, because we restrict the initial data to modulated binary oscillations. However, they can produce reasonable results only for sufficiently small times: If the first macroscopic wave arrives at the boundary of the computational domain, we shall stop the numerical computations.

Example $R1$

Here we study the evolution of cold initial data with a single jump discontinuity. In particular we set $v^{\text{odd}}(\overline{\alpha}) = v^{\text{even}}(\overline{\alpha}) = 0$, and

$$r^{\text{odd}}(\overline{\alpha}) \;=\; r^{\text{even}}(\overline{\alpha}) \;=\; \begin{cases} 0 & \text{falls} \quad \overline{\alpha} < 0.5, \\ 1 & \text{falls} \quad \overline{\alpha} \geq 0.5. \end{cases}$$

The resulting atomic data are depicted in Figure 27, where all computations are

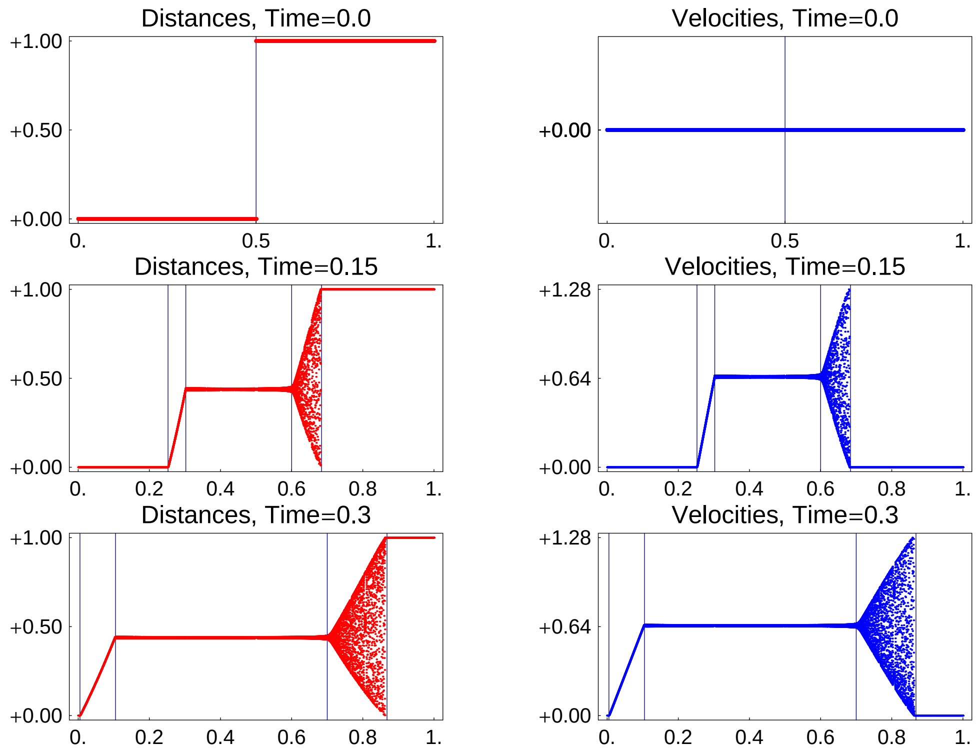

Figure 27: The atomic distances and velocities for Example $R1$ with $\overline{t} = 0.0$, $\overline{t} = 0.15$ and $\overline{t} = 0.3$. The vertical lines separate waves from constant states. ⋄

carried out for 16000 particles. The results can be interpreted as follows:

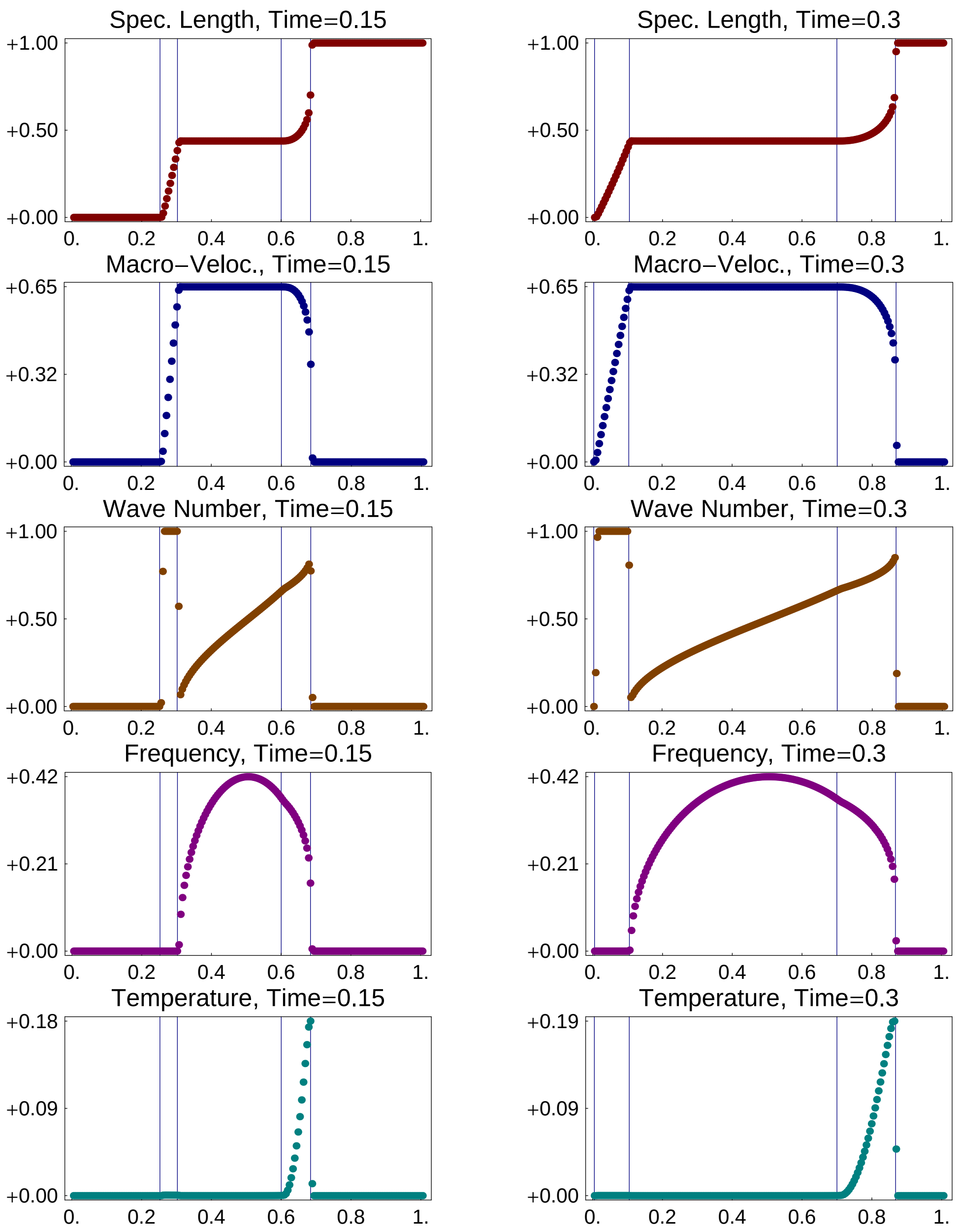

Figure 28: Various macroscopic fields for Example $R1$ (for fixed macroscopic times as function of $\overline{\alpha}$). Vertical lines again separate waves from constant states. $\diamond$

1. There is a cold rarefaction wave, which runs to the left. On the left hand side of this wave no microscopic motion can be observed on the macroscopic scale.

2. We find a second, right going wave, which has a head and a rear front. Within this wave the motion generates microscopic oscillations, but there are no oscillations outside this wave.

3. Between the two waves there appears a new constant state with cold data.

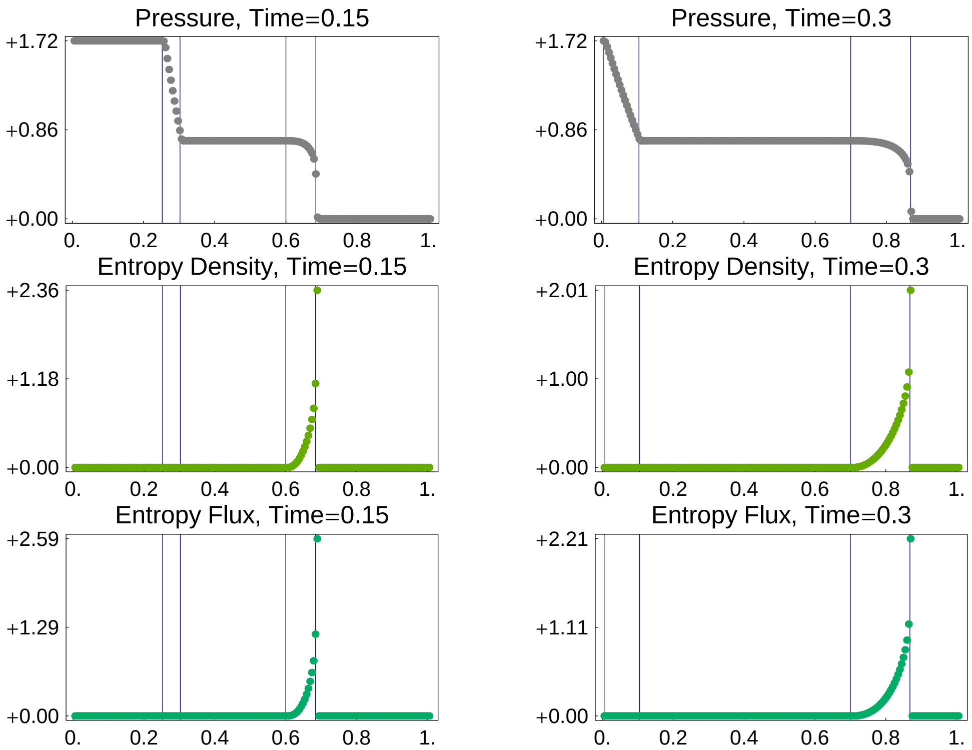

Figure 29: see Figure 28. ◇

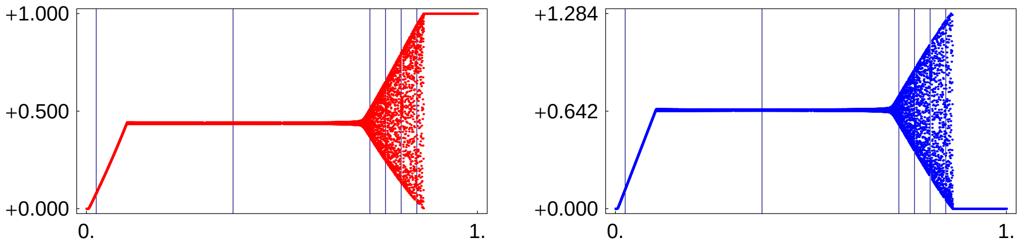

Figure 30: The vertical lines mark the $\overline{\alpha}$-coordinate of the macroscopic points, for which we evaluate the microscopic distribution functions in Figure 31. There holds $\overline{t} = 0.3$. ◇

N	=	16000			
ma_final_time	=	3.0E-01	mi_final_time	=	4.8E+03
mi_time_delta	=	4.0E-03	mi_time_steps	=	1200000
mv_win_t_len	=	9486	mv_win_p_len	=	80
df_win_t_len	=	9486	df_win_p_len	=	126
df_win_prm	=	100			

Table 8: Numerical parameters for Example $R1$. ◇

Note that our concept of waves is borrowed from the theory of hyperbolic pde's, so that every wave connects two constant states. In particular, we interpret the region with temperature as a single wave with head and rear front.

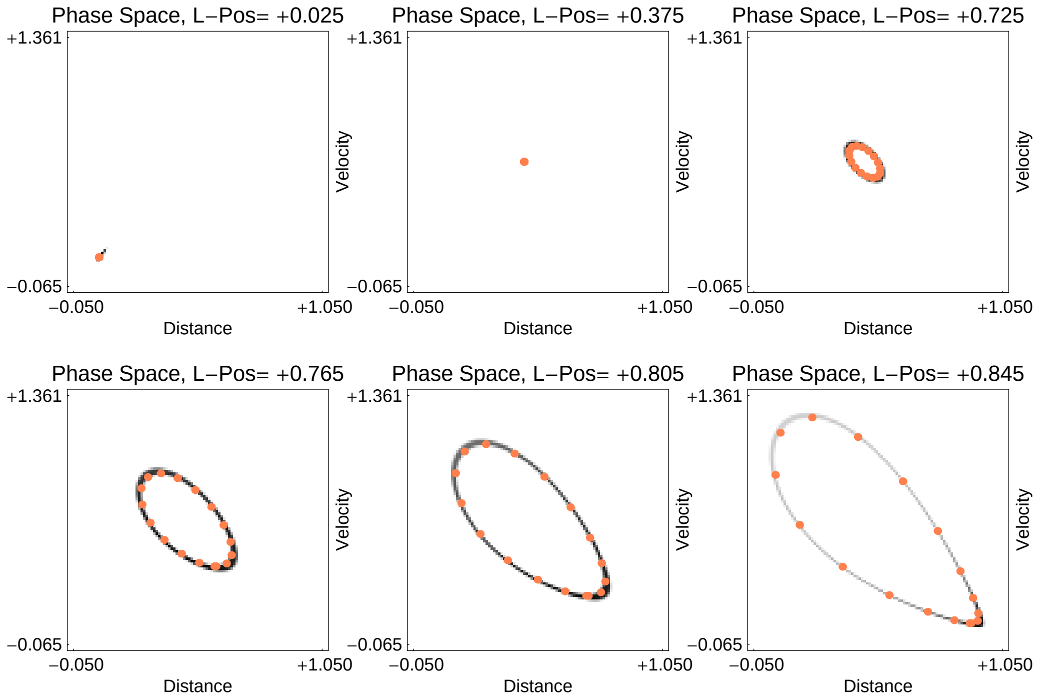

Figure 31: Local distribution functions in the microscopic phase space for Example $R1$, evaluated in the macroscopic points from Figure 30: Gray and Orange correspond to microscopic distributions and macroscopic predictions, respectively. ⋄

Figures 28 and 29 show various macroscopic fields, and allow the following interpretations:

1. All macroscopic fields exhibit self similar profiles, i.e. they depend only on $\overline{c} := (\overline{\alpha} - 0.5)/\overline{t}$.

2. Within the constant state between the waves we find non-constant values for wave number and frequency. However, this values have no physical meaning, because the temperature vanishes in this region. Similarly, there is no reasonable interpretation for the jump of wave number in the first wave.

3. Within the second wave, the temperature T as well as the entropy S increase with $\overline{c}$. Finally, at the head front of the second wave, both fields jump back to zero.

4. All macroscopic fields exhibit the same qualitative behavior, i.e. there are smooth within the second wave, continuous at the rear front, but discontinuous at the head front. In the context of hyperbolic systems such waves are called *composite waves*.

In Figure 30 we fix six macroscopic points at $\overline{t} = 0.3$ for which we compare in Figure 31 the microscopic distribution functions with their macroscopic predictions. Again we observe a perfect coincidence between microscopic distribution functions and macroscopic predictions. Thus we conclude that the microscopic oscillations are in fact given by modulated traveling waves.

The appearance of composite waves contradicts the classical LAX-Theory for regular hyperbolic systems (which means the system is strictly hyperbolic and all eigenvalues are either linearly degenerate or genuinely nonlinear). According to this theory there should be another constant state separating the rarefaction fan from the jump discontinuity. Up to now there is no satisfactory explanation for the appearance of composite waves, because we expect the modulation system to be regular in the sense from above. However, we think that the appearance of composite waves is caused by the fact, that the modulation system is not fully satisfied across the jump discontinuity. To be more precise, we think that it is impossible to find *four* independent jump conditions which are satisfied across the shock[2]. If this conjecture is right, the composite wave cannot be explained within the classical theory for hyperbolic systems.

[2]We have no doubt that the jump conditions of mass, momentum and energy are satisfied, but we believe that there holds no further jump condition.

Example $R2$

In this example we study the contact problem between a cold state and a binary oscillation. To initialize the chain we choose $v^{\text{odd}}(\overline{\alpha}) = v^{\text{even}}(\overline{\alpha}) = 0$ and

$$r^{\text{odd}}(\overline{\alpha}) = \begin{cases} -1 & \text{falls } \overline{\alpha} < 0.5, \\ +1 & \text{falls } \overline{\alpha} \geq 0.5, \end{cases}$$
$$r^{\text{even}}(\overline{\alpha}) = \begin{cases} +3 & \text{falls } \overline{\alpha} < 0.5, \\ +1 & \text{falls } \overline{\alpha} \geq 0.5. \end{cases}$$

Figure 32 shows the atomic data for $N = 4000$ at the macroscopic times $\overline{t} = 0.0$,

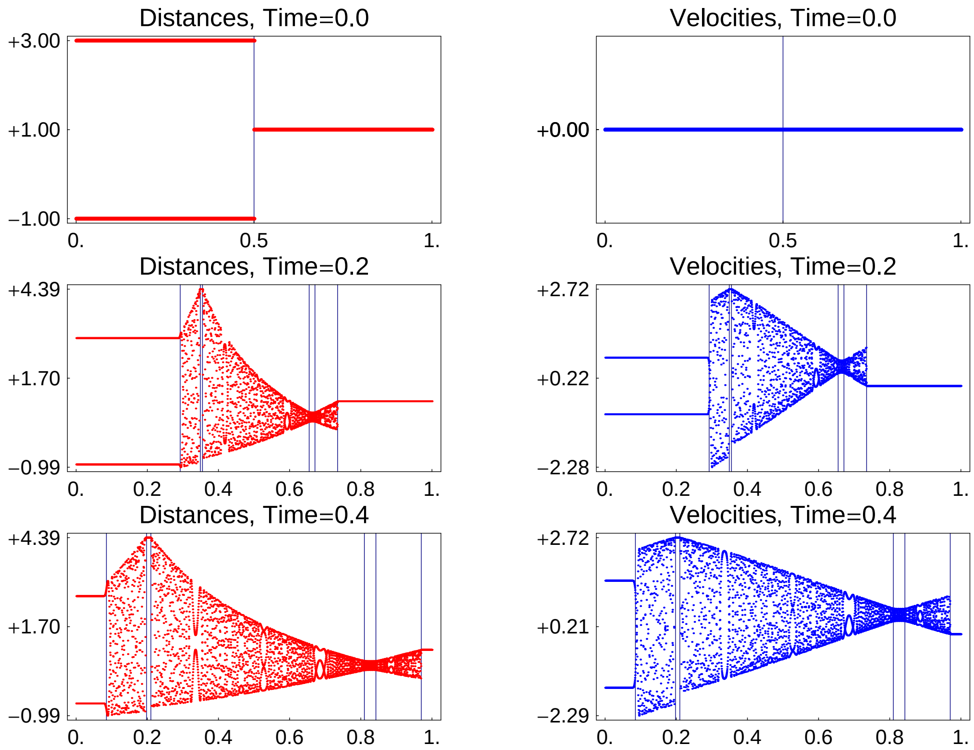

Figure 32: The atomic distances and velocities for Example $R2$, depicted for $\overline{t} = 0.0$, $\overline{t} = 0.2$ and $\overline{t} = 0.4$. The vertical lines separate waves from constant states. $\diamond$

N	=	4000			
ma_final_time	=	4.0E-01	mi_final_time	=	1.6E+03
mi_time_delta	=	1.0E-02	mi_time_steps	=	160000
mv_win_t_len	=	2529	mv_win_p_len	=	10
df_win_t_len	=	2529	df_win_p_len	=	20
df_win_prm	=	100			

Table 9: Numerical parameters for Example $R2$. $\diamond$

$\overline{t} = 0.2$ and $\overline{t} = 0.4$. We observe the creation of three waves each with two fronts:

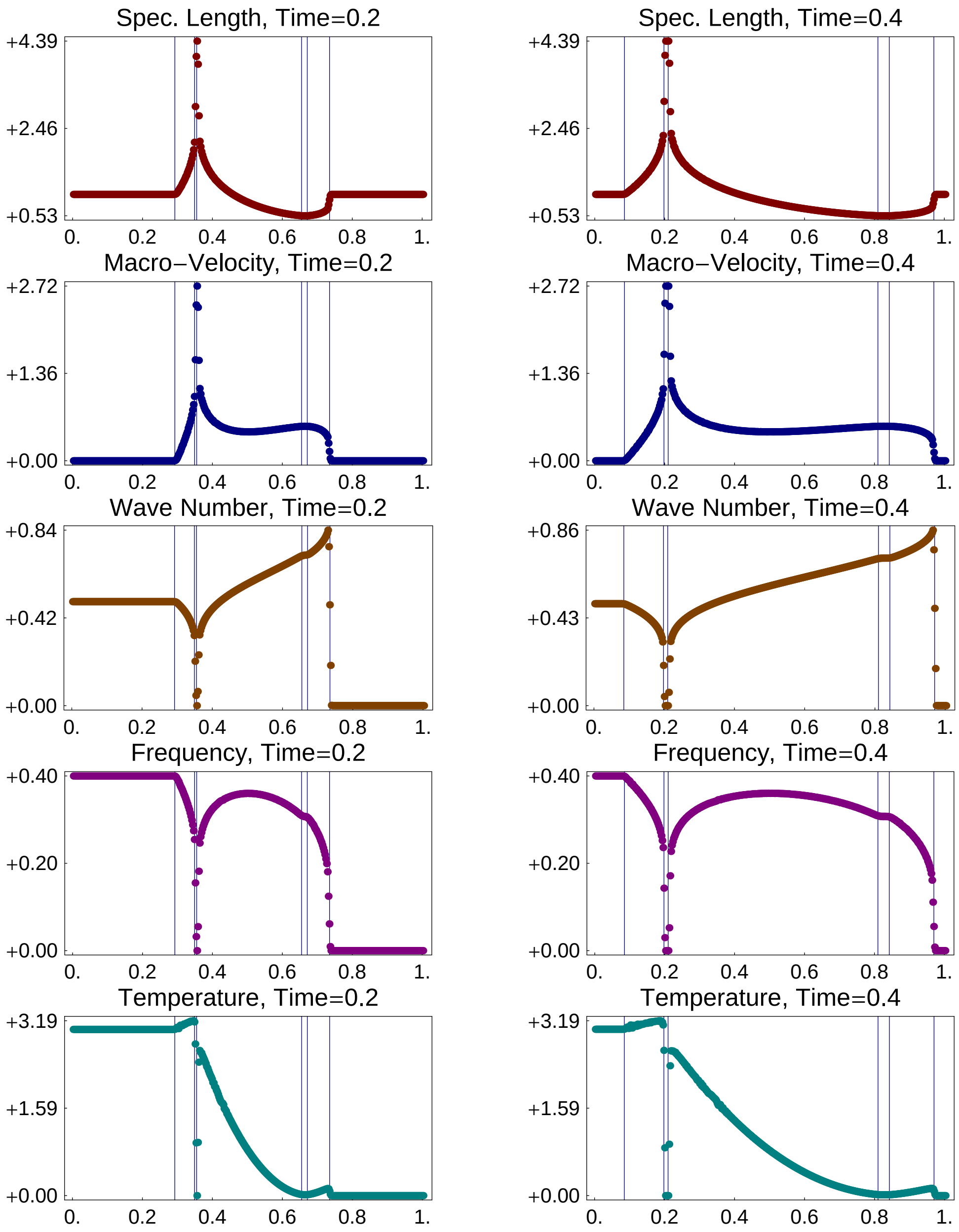

Figure 33: Various macroscopic fields for Example $R2$ with $\overline{t} = 0.2$ and $\overline{t} = 0.4$. The vertical lines separate waves from constant states. $\diamond$

The first wave runs to the left, the second wave spreads out both to the left and to the right, and the third wave goes to the right. There is a constant state between the second and the third wave, whereas the width of the constant state between the first two waves is almost zero. However, the transition between the first and the second wave can be read off from the envelopes of the microscopic oscillations.

We have depicted the profiles of various macroscopic fields in Figure 33. Again we observe self similarity, so that all macroscopic fields depend only on $\overline{c} = (\overline{\alpha} - 0.5)/\overline{t}$.

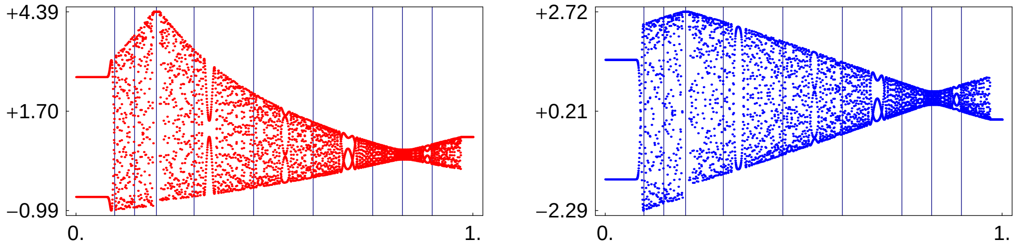

Figure 34: The vertical lines mark the $\overline{\alpha}$-coordinate of the macroscopic points, for which we evaluate the microscopic distribution functions in Figure 35. There holds $\overline{t} = 0.4$. $\diamond$

Due to the qualitative behavior of these profiles we classify all three waves as composite waves.

By construction, the third waves contacts a region with zero temperature. Surprisingly, the same is right for the first two waves, because the temperature vanishes in the constant state in between. In particular, the temperature increases with $\overline{c}$ within the first wave, then it jumps to zero, jumps back to a positive value, and finally it decreases with $\overline{c}$ within the second wave. A similar qualitative behavior can be observed for all other macroscopic fields.

In Figure 35 we compare microscopic distribution functions and their macroscopic predictions in nine selected macroscopic points, which cover all three waves, see Figure 34. Again we find a perfect matching between the microscopic and the macroscopic data.

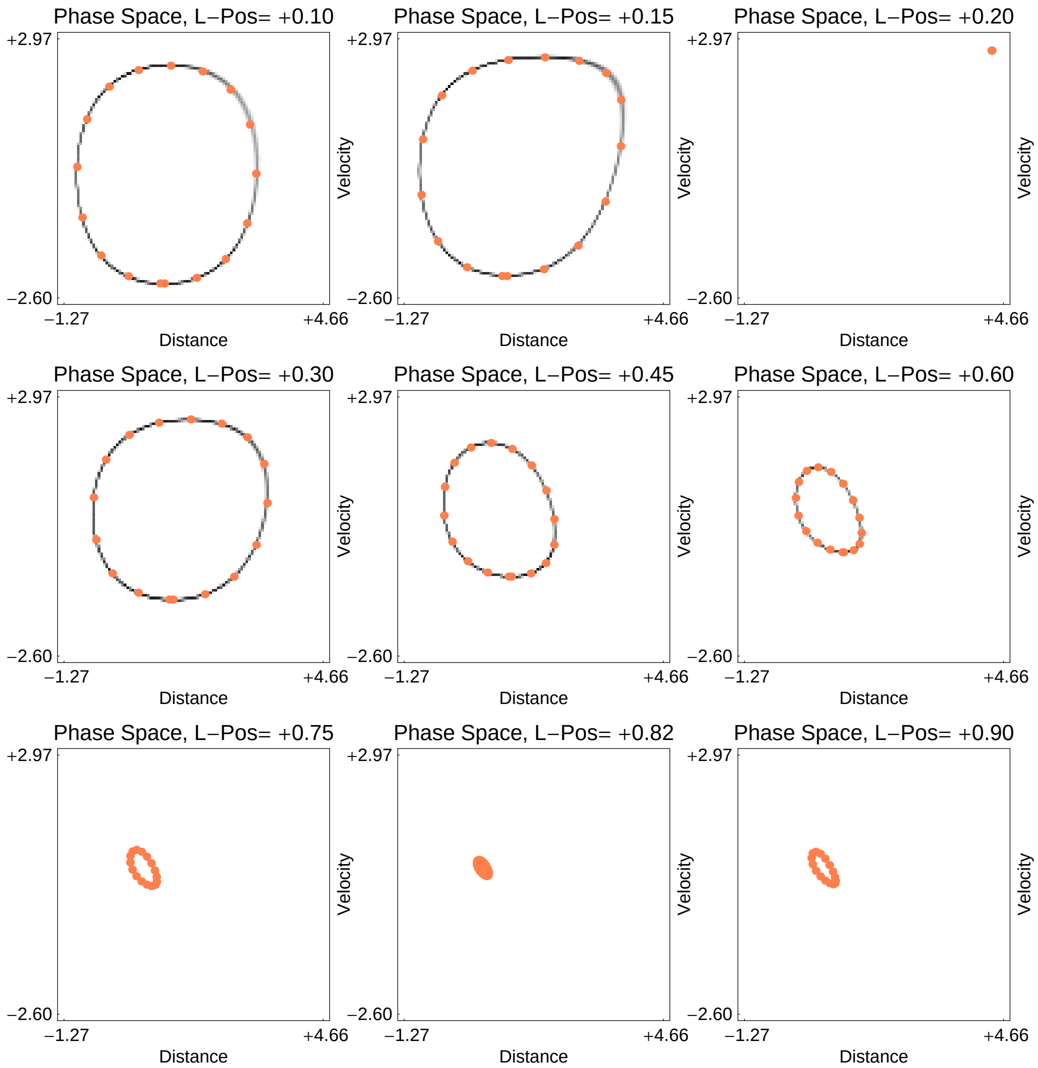

Figure 35: Local distribution functions in the microscopic phase space for Example $R2$, evaluated in the macroscopic points from Figure 34: Gray and Orange correspond to microscopic distributions and macroscopic predictions, respectively. $\diamond$

Example $R3$

In this example we consider a RIEMANN-problem with oscillating data at both sides of the initial jump. We set $v^{\text{odd}}(\overline{\alpha}) = v^{\text{even}}(\overline{\alpha}) = 0$ and

$$r^{\text{odd}}(\overline{\alpha}) = \begin{cases} 0 & \text{falls} \quad \overline{\alpha} < 0.38, \\ 2 & \text{falls} \quad \overline{\alpha} \geq 0.38, \end{cases}$$
$$r^{\text{even}}(\overline{\alpha}) = \begin{cases} 1 & \text{falls} \quad \overline{\alpha} < 0.38, \\ 3 & \text{falls} \quad \overline{\alpha} \geq 0.38, \end{cases}$$

so that the initial jump is located at $\overline{\alpha} = 0.38$. There resulting atomic data for

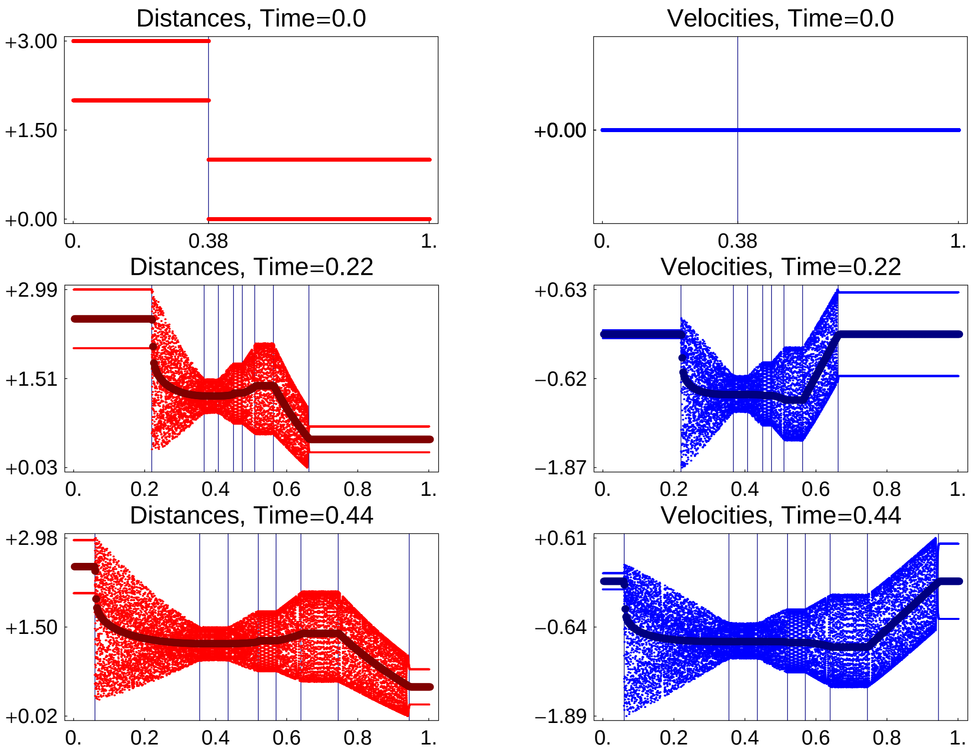

Figure 36: The atomic distances and velocities for Example $R3$, depicted for $\overline{t} = 0.0$, $\overline{t} = 0.22$ and $\overline{t} = 0.44$. The vertical lines separate waves from constant states. $\diamond$

`N`	=	`16000`			
`ma_final_time`	=	`4.4E-01`	`mi_final_time`	=	`7.04E+03`
`mi_time_delta`	=	`2.0E-02`	`mi_time_steps`	=	`352000`
`mv_win_t_len`	=	`2782`	`mv_win_p_len`	=	`40`
`df_win_t_len`	=	`475`	`df_win_p_len`	=	`1`
`df_win_prm`	=	`100`			

Table 10: Numerical parameters for Example $R3$. $\diamond$

$N = 16000$ are represented in Figure 36, and Figure 37 contains the corresponding

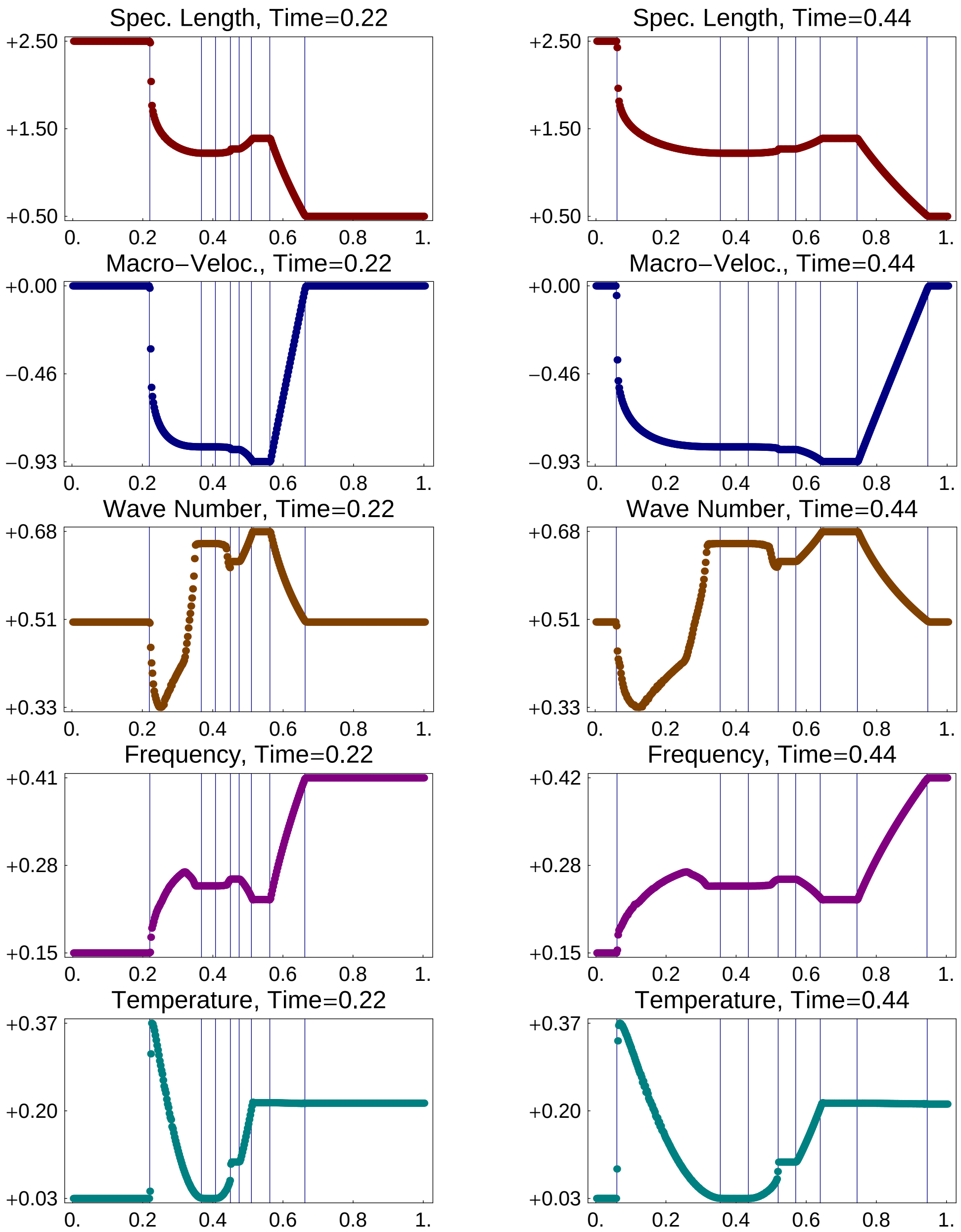

Figure 37: Various macroscopic fields for Example $R3$ with $\bar{t} = 0.22$ and $\bar{t} = 0.44$. The vertical lines separate waves from constant states. $\diamond$

profiles of $N = 16000$ various macroscopic fields. We can identify four consecutive waves, which all are separated by constant states. At first we study the third and the fourth wave, which we classify as rarefaction waves. Note that the temperature remains constant within the fourth wave. We choose nine macroscopic points behind the second wave, see Figure 38, and compare the microscopic distributions with their macroscopic predictions. The results are presented in Figure 39. We observe a perfect matching between microscopic and macroscopic data, and we conclude that the microscopic oscillations in this region are again determined by modulated

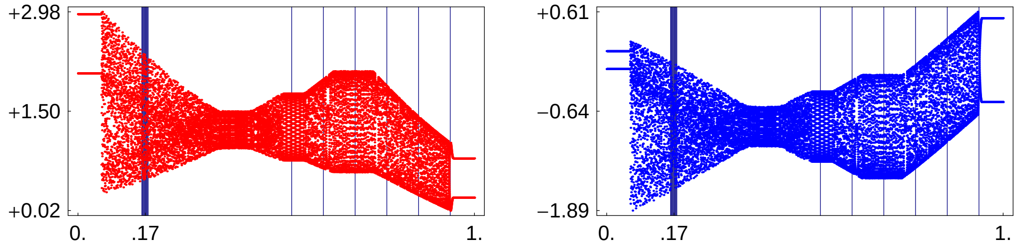

Figure 38: The vertical lines mark the $\overline{\alpha}$-coordinate of the macroscopic points, for which we evaluate the microscopic distribution functions, see Figures 39 and 40. There holds $\bar{t} = 0.44$. $\diamond$

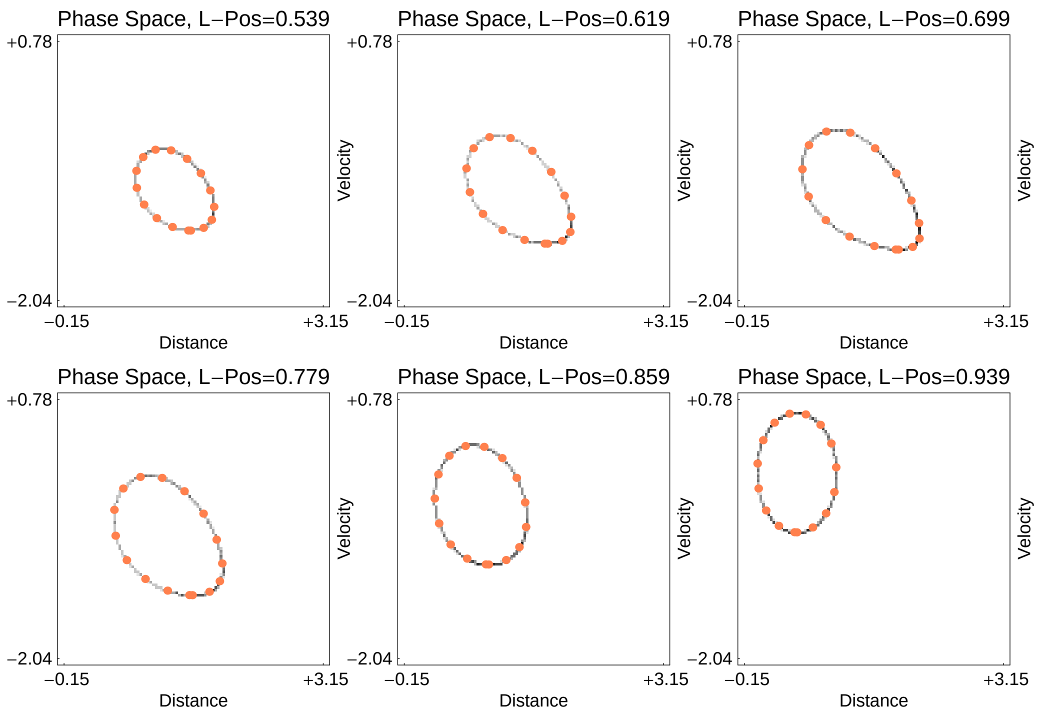

Figure 39: Local distribution functions in the microscopic phase space for Example $R3$, evaluated for six macroscopic points **behind the second wave**, cf. Figure 38. Gray and Orange correspond to microscopic distributions and macroscopic predictions, respectively. **Interpretation**: The microscopic oscillations in this region can be described by modulated traveling waves. $\diamond$

traveling waves.

The microscopic oscillations within the first two waves cannot be described by modulated traveling waves, so that here the modulation theory fails. To justify this assertion we shall consider Figure 40, where we compare again microscopic distributions with their macroscopic predictions. This comparison is carried out in nine macroscopic points, which are very close to each other, so that the macroscopic predictions almost coincide.

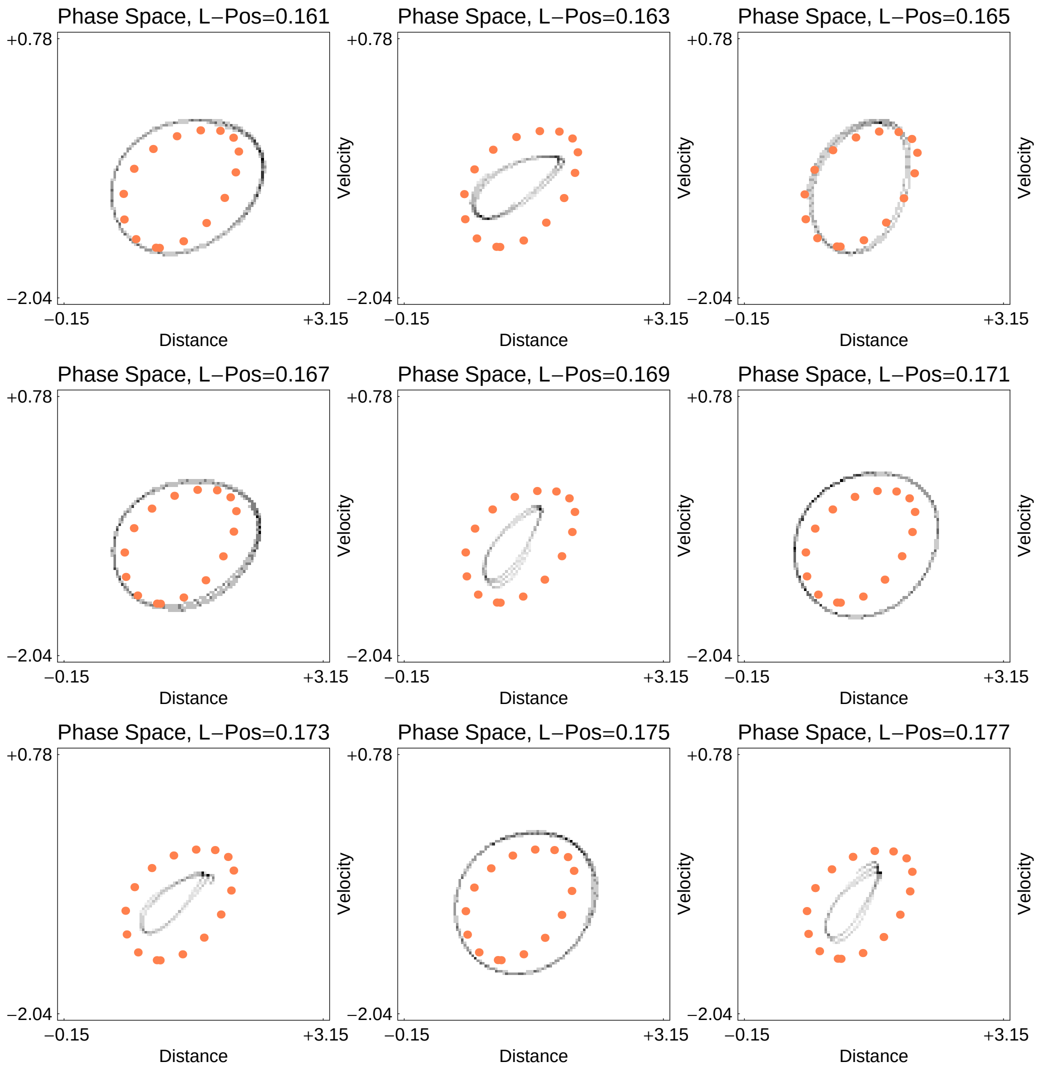

Figure 40: Local distribution functions in the microscopic phase space for Example $R3$, evaluated in the neighborhood of the macroscopic point $\left(\overline{t} = 0.44,\, \overline{\alpha} = 0.17\right)$, cf. Figure 38. Gray and Orange as in Figure 39. Note that all distribution functions describe the temporal statistics of a **single particle**. **Interpretation**: The microscopic distributions oscillate around the macroscopic predictions. ◇

In contrast to the preceding examples, here the underlying space-time windows contain only one particle. Therefore, all microscopic distributions in Figure 40 describe the temporal statistics of a single particle. These one-particle distributions do no longer equal the macroscopic predictions: The distribution functions rather oscillate around the macroscopic predictions. We mention that the same behaviour can be found within the second wave.

The data from Figure 40 suggest, that every one-particle distribution function is still determined by a traveling wave. However, these traveling waves now vary on the microscopic scale. We thus suppose, that the microscopic oscillations within the first wave should be described in terms of WIGNER-measures, which allow the fast modulation of wave number and frequency. We mention that WIGNER-measures provide a complete and rigorous description of the thermodynamic limit for the harmonic chain. For the details we refer to [Mac02, Mac03, Mie05]

4 Conclusions

In the previous section we have studied the validity of modulation theory, and have observed the following phenomena:

1. If all macroscopic fields are smooth, the oscillations in the atomic data can be described in terms of modulated traveling waves, and the macroscopic dynamics is governed by the modulation system (6).

2. Moreover, we can use modulated traveling wavesto describe the microscopic oscillations, which emerge when cold data evolve shocks.

3. If the shocks evolve from data with temperature, the microscopic oscillations exhibit a more complicated structure, and modulation theory fails in this case.

Recall that these propositions are valid only under the following restrictions:

(i) The interaction potential Φ is convex.

(ii) The macroscopic scale results from the hyperbolic scaling (4).

(iii) The initial data are given in form of modulated binary oscillations or, more general, in form of modulated traveling waves.

All in all we can conclude that the modulation theory provides the right thermodynamic description for a wide class of problems. In particular, the theory is able to describe the creation of temperature from cold data as well as the transport of heat in a nonlinear medium.

However, the macroscopic system (6) is not completely understood, because all properties of (6) are determined by the equation of state $U = U(r, k, S)$. This equation of state depends on the interaction potential Φ, and is almost never given explicitly. For that reason we cannot characterize the macroscopic solutions of (6) without relying on the corresponding microscopic solution of NEWTON's equations (2). In particular, it remains a challenging problem to find a macroscopic theory that describes the solutions of RIEMANN problems.

Acknowledgement. We like to thank Alexander Mielke for several fruitful discussions.

References

[AG96] G. Arioli and F. Gazzola, *Periodic motion of an infinite lattice of particles with nearest neighbor interaction*, Nonl. Anal. TMA **26** (1996), no. 6, 1103–1114.

[DH05] W. Dreyer and M. Herrmann, *On the approximation of periodic traveling waves for the atomic chain*, WIAS preprint 1030, 2005.

[DHM04] W. Dreyer, M. Herrmann, and A. Mielke, *Micro-macro transitions for the atomic chain via Whitham's modulation equation*, WIAS preprint 1032, 2004.

[DKKZ96] P. Deift, S. Kamvissis, T. Kriecherbauer, and X. Zhou, *The Toda rarefaction problem*, Comm. Pure Appl. Math **49** (1996), no. 1, 35–83.

[DM98] P. Deift and T. T-R McLaughlin, *A continuum limit of the Toda lattice*, Mem. Americ. Math. Soc., vol. 131/624, Americican Mathematical Society, 1998.

[FP99] G. Friesecke and R. L. Pego, *Solitary waves on FPU lattices. I. Qualitative properties, renormalization and continuum limit*, Comm. Math. Phys. **12** (1999), no. 6, 1601–1627.

[FV99] A.-M. Filip and S. Venakides, *Existence and modulation of traveling waves in particle chains*, Comm. Pure Appl. Math. **51** (1999), no. 6, 693–735.

[FW94] G. Friesecke and J. A. D. Wattis, *Existence theorem for solitary waves on lattices*, Comm. Math. Phys. **161** (1994), no. 2, 391–418.

[GM04a] J. Giannoulis and A. Mielke, *Macroscopic dynamics of an oscillator chain by the nonlinear Schrödinger equation*, AMSMSP-Preprint 117, 2004.

[GM04b] J. Giannoulis and A. Mielke, *The nonlinear Schrödinger equation as a macroscopic limit for an oscillator chain with cubic nonlinearities*, Nonlinearity **17** (2004), 551–565.

[Hén74] M. Hénon, *Integrals of the Toda lattice*, Phys. Rev. B **9** (1974), no. 4, 1921–1923.

[Her04] M. Herrmann, *Ein Mikro-Makro-Übergang für die nichtlineare atomare Kette mit temperatur*, Doctoral thesis, Humboldt-Universität zu Berlin, 2004.

[HFM81] B.L. Holian, H. Flaschka, and D.W. McLaughlin, *Shock waves in the toda lattice: Analysis*, Phys. Rev. A **24** (1981), no. 5, 2595–2623.

[HLM94] M.H. Hays, C. D. Levermore, and P.D. Miller, *Macroscopic lattice dynamics*, Physica D **79** (1994), no. 1, 1–15.

[HLW02] E. Hairer, Ch. Lubich, and G. Wanner, *Geometric Numerical Integration*, Springer Series in Computational Mathematics, vol. 31, Springer-Verlag, Berlin, 2002.

[HS78] B. L. Holian and G. K. Straub, *Molecular dynamics of shock waves in one–dimensional chains*, Phys. Rev. B **18** (1978), 1593.

[Kam91] S. Kamvissis, *On the long time behavior of the double infinite toda chain under shock initial data*, Ph.D. thesis, New York University, 1991.

[Mac02] F. Maciá, *Propagación y control de vibraciones en medios discretos y continous*, Ph.D. thesis, Universidad Complutense de Madrid, Dept. de Matem, Aplicada, 2002.

[Mac03] ———, *Wigner measures in the discrete setting: high-frequency analysis of sampling & reconstruction operators*, 2003.

[Mie05] A. Mielke, *Macroscopic behavior of microscopic oscillations in harmonic lattices using wigner-husimi measures*, Preprint, 2005.

[PP00] A. A. Pankov and K. Pflüger, *Traveling waves in lattice dynamical systems*, Math. Meth. Appl. Sci. **23** (2000), 1223–1235.

[SW00] G. Schneider and C. E. Wayne, *Counter-propagating waves on fluid surfaces and the continuum limit for the Fermi-Pasta-Ulam model*, International Conference on Differential Equations, vol. 1, World Scientific, 2000, pp. 390–404.

[SYS97] R. D. Skeel, G. Yang, and T. Schlick, *A family of symplectic integrators: Stability, accuracy, and molecular dynamics Applications*, SIAM J. Sci. Comput. **18** (1997), 203–222.

[Tod70] M. Toda, *Waves in nonlinear lattices*, Prog. Theor. Phys. **45** (1970), 174–200.

[Tod81] ———, *Theory of nonlinear lattices*, Springer Series in Solid-State Sci., vol. 20, Springer, Berlin, 1981.

[VDO91] S. Venakides, P. Deift, and R. Oba, *The Toda shock problem*, Comm. Pure Appl. Math. (1991), 1171–1242.

[Whi74] G. B. Whitham, *Linear and Nonlinear Waves*, Pure And Applied Mathematics, vol. 1237, Wiley Interscience, New York, 1974.